Brain motor and fear circuits regulate leukocytes during acute stress

Wolfram C. Poller[1,2,✉], **Jeffrey Downey**[1,2,3,4,5], **Agnes A. Mooslechner**[2], **Nargis Khan**[3,4,5], **Long Li**[6], **Christopher T. Chan**[1,2], **Cameron S. McAlpine**[1,2,6], **Chunliang Xu**[7], **Florian Kahles**[2], **Shun He**[2], **Henrike Janssen**[1,2], **John E. Mindur**[2], **Sumnima Singh**[1,2], **Máté G. Kiss**[1,2], **Laura Alonso-Herranz**[2], **Yoshiko Iwamoto**[2], **Rainer H. Kohler**[2], **Lai Ping Wong**[8,9], **Kashish Chetal**[8,9], **Scott J. Russo**[6], **Ruslan I. Sadreyev**[8,9], **Ralph Weissleder**[2,10], **Matthias Nahrendorf**[2], **Paul S. Frenette**[7,11], **Maziar Divangahi**[3,4,5], **Filip K. Swirski**[1,2,✉]

[1]Cardiovascular Research Institute, Icahn School of Medicine at Mount Sinai, New York, NY, USA.

[2]Center for Systems Biology and Department of Radiology, Massachusetts General Hospital and Harvard Medical School, Boston, MA, USA.

[3]Department of Medicine, McGill University Health Centre, McGill International TB Centre, Meakins-Christie Laboratories, McGill University, Montreal, Quebec, Canada.

[4]Department of Microbiology & Immunology, McGill University Health Centre, McGill International TB Centre, Meakins-Christie Laboratories, McGill University, Montreal, Quebec, Canada.

[5]Department of Pathology, McGill University Health Centre, McGill International TB Centre, Meakins-Christie Laboratories, McGill University, Montreal, Quebec, Canada.

[6]Nash Family Department of Neuroscience, Friedman Brain Institute, Icahn School of Medicine at Mount Sinai, New York, NY, USA.

[7]The Ruth L. and David S. Gottesman Institute for Stem Cell and Regenerative Medicine Research, Albert Einstein College of Medicine, New York, NY, USA.

[8]Department of Molecular Biology, Massachusetts General Hospital and Harvard Medical School, Boston, MA, USA.

[9]Department of Pathology, Massachusetts General Hospital and Harvard Medical School, Boston, MA, USA.

[10]Department of Systems Biology, Harvard Medical School, Boston, MA, USA.

[11]Deceased: Paul S. Frenette.

Abstract

The nervous and immune systems are intricately linked[1]. Although psychological stress is known to modulate immune function, mechanistic pathways linking stress networks in the brain to peripheral leukocytes remain poorly understood[2]. Here we show that distinct brain regions shape leukocyte distribution and function throughout the body during acute stress in mice. Using optogenetics and chemogenetics, we demonstrate that motor circuits induce rapid neutrophil mobilization from the bone marrow to peripheral tissues through skeletal-muscle-derived neutrophil-attracting chemokines. Conversely, the paraventricular hypothalamus controls monocyte and lymphocyte egress from secondary lymphoid organs and blood to the bone marrow through direct, cell-intrinsic glucocorticoid signalling. These stress-induced, counter-directional, population-wide leukocyte shifts are associated with altered disease susceptibility. On the one hand, acute stress changes innate immunity by reprogramming neutrophils and directing their recruitment to sites of injury. On the other hand, corticotropin-releasing hormone neuron-mediated leukocyte shifts protect against the acquisition of autoimmunity, but impair immunity to SARS-CoV-2 and influenza infection. Collectively, these data show that distinct brain regions differentially and rapidly tailor the leukocyte landscape during psychological stress, therefore calibrating the ability of the immune system to respond to physical threats.

How the central nervous system might control leukocytes during acute stress has previously been surmised[2], but there has been little focus on the processes that link brain networks with leukocyte dynamics. To investigate this, we exposed mice to different acute stressors, including restraint (Fig. 1a). Within 1 h of exposure, we observed a decrease in the numbers of circulating monocytes and lymphocytes and an increase in the number of neutrophils (Fig. 1a and Extended Data Fig. 1a). To assess the kinetics of these changes, we performed time-course experiments. We observed two distinct patterns in the blood—whereas lymphocyte and monocyte numbers diminished gradually and returned to the baseline during stress recovery, neutrophil numbers increased quickly and sharply returned to the baseline (Fig. 1b). Less numerous leukocyte types behaved similarly to lymphocytes and monocytes (Extended Data Fig. 1b). Restraint stress of only 30 s was sufficient to induce peak neutrophilia, albeit after a 1 h delay, but maximal monocytopenia and lymphopenia required at least 4 h of restraint (Fig. 1b and Extended Data Fig. 1c). We confirmed these data using intravital microscopy (Fig. 1c). Thus, in response to restraint, we observed an early period of opposing leukocyte flux characterized by lymphopenia and monocytopenia on the one hand, and neutrophilia on the other.

Fluctuating cell numbers in the blood during acute stress motivated us to characterize the tissue destination and source of the leukocytes. First, we found that acute stress diverted lymphocytes and monocytes out of peripheral organs and sequestered them in the bone marrow (Fig. 1d), where they resided temporarily (Fig. 1e and Extended Data Fig. 1d). Given the importance of secondary lymphoid organs to immunity, we enumerated B and T cells in the lymph nodes and spleen and, similarly, observed a substantial lymphocyte reduction, consistent with redistribution to the bone marrow, followed by a protracted return (Fig. 1f). Even 40 h of recovery was insufficient to replenish the secondary lymphoid organs to pre-stress numbers. We found a similar pattern among other leukocytes (Extended Data Fig. 1e).

Second, we focused on neutrophils. The spleen was not a relevant reservoir (Extended Data Fig. 1f) and the bone marrow did not trigger emergency haematopoiesis (Extended Data Fig. 1g), which was expected given the speed of the response[3]. Using cell tracking, we found that acute stress mobilized neutrophils out of the bone marrow (Fig. 1g). Taking into account the predicted number of all neutrophils residing throughout all bone marrow in the body[4,5], we estimated that the total loss of endogenous neutrophils from the bone marrow was similar to, if not greater than, their total gain in various peripheral destinations (Fig. 1g). These data show that acute psychological stress rapidly induces large-scale whole-body redistribution of all major leukocytes.

The role of the HPA axis in acute stress

We next sought to elucidate the pathways through which the brain controls peripheral leukocyte dynamics. We started by testing the hypothalamic–pituitary–adrenal (HPA) axis and the sympathetic nervous system (SNS)[6]. Adrenalectomy, which ablated corticosterone release in stressed mice (Extended Data Fig. 2a), abrogated the decrease in lymphocytes and monocytes in the blood (Fig. 2a), whereas injecting corticosterone into control animals (Extended Data Fig. 2b) reduced cell numbers (Fig. 2b), indicating that the HPA axis was modulating these populations. To determine whether the HPA axis acted directly on leukocytes through the glucocorticoid receptor (GR) nuclear receptor subfamily 3, group C, member 1 (NR3C1) (Extended Data Fig. 2c), we generated mice lacking NR3C1 in specific leukocytes. We found that the effects were leukocyte intrinsic (Fig. 2c–e and Extended Data Fig. 2d,e). As CXCR4 is a bone marrow retention and homing factor that is regulated by glucocorticoids[7–11], we wondered whether lymphocytes and monocytes used this chemokine receptor. Indeed, B and T cells and monocytes augmented *Cxcr4* expression during stress (Fig. 2f), and CXCR4 inhibition blocked the transit of the cells to the bone marrow (Fig. 2g). These data suggest that the HPA axis controls the stress-induced migration of lymphocytes and monocytes from peripheral tissues and the blood to the bone marrow through leukocyte-intrinsic corticosterone-mediated augmentation of CXCR4.

To understand how the brain controls HPA axis-mediated leukocyte migration into the bone marrow during acute stress, we turned our attention to the paraventricular hypothalamus (PVH), which is active during acute stress, as indicated by the neuronal activation marker FOS[12,13] (Fig. 2h). First, we chemogenetically stimulated CRH neurons in the PVH of *Crh^cre* mice[14] (Extended Data Fig. 3a). Compared with the controls, activation of

corticotropin-releasing hormone (CRH) neurons in this brain region increased peripheral corticosterone and strongly decreased lymphocytes and monocytes in the blood (Fig. 2i and Extended Data Fig. 3b–d), an effect that depended on the adrenal glands (Extended Data Fig. 3e). Second, we performed the converse experiment by injecting an adeno-associated virus encoding Cre-dependent expression of Caspase-3[15] into the PVH of *Crh^cre* mice (Extended Data Fig. 3f). When stressed, mice lacking CRH neurons showed an abrogated corticosterone response and no more decrease in B cells, T cells or monocytes (Fig. 2j). Third, we deleted the *Crh* gene from hypothalamic neurons by crossing *Crh^fl/fl* mice with *Sim1^cre* mice and detected neither elevated corticosterone levels nor reduced B cells, T cells or monocytes in the blood during stress, highlighting that the neuropeptide CRH rather than the projections of CRH neurons to downstream sites[16,17] induces leukocyte shifts (Fig. 2k). We also examined how blood neutrophils were affected and concluded that the PVH was not required for inducing neutrophilia; on the contrary, the PVH strongly blunted neutrophilia (Extended Data Fig. 3g). Thus, the PVH–CRH axis is required for the reduction and bone marrow homing of circulating B cells, T cells and monocytes during acute stress.

Central motor circuits and neutrophilia

We next sought to determine which of the brain's output systems was responsible for stress-induced neutrophilia. We hypothesized that the SNS was the probable culprit as it has a crucial role in leukocyte mobilization[18–20]. Thus, we performed a series of gain- and loss-of-function experiments. First, ablating the SNS had no effect on acute-stress-induced neutrophilia (Extended Data Fig. 4a). Second, neither pharmacologically blocking (Extended Data Fig. 4b) nor genetically deleting adrenoceptors (Extended Data Fig. 4c) blunted neutrophilia. Third, whereas only artificially high doses of noradrenaline (Extended Data Fig. 4d) led to neutrophilia, adrenalectomy did not eliminate it (Extended Data Fig. 4e). Fourth, neutrophilia persisted in the absence of IL-6 (ref.[21]) (Extended Data Fig. 4f). Finally, we found that optogenetically stimulating catecholaminergic neurons in the rostroventrolateral medulla[22,23] did not induce neutrophilia (Extended Data Fig. 4g). These data indicate that, despite the role of the SNS in accelerating haematopoiesis during chronic variable stress[18], neutrophilia induced by acute restraint stress was SNS independent.

The finding that neutrophilia induced by acute stress was SNS independent necessitated a different strategy. We measured a series of possible neutrophil modulators in the blood after restraint. Among them, two were increased (Fig. 3a), one of which was IL-16, which was present at low levels (Fig. 3b). The other was CXCL1, which is known to mobilize neutrophils[24–26], and which was abundantly present (Fig. 3c). The CXCL1 increase in the serum temporally correlated with blood neutrophilia (Fig. 3d), whereas an inhibitor of its receptor CXCR2[27] abrogated neutrophilia (Fig. 3e) and recombinant CXCL1 induced it (Extended Data Fig. 4h). These data led us to identify the source of CXCL1 during restraint stress. Among the tissues, skeletal muscle showed the most augmented *Cxcl1* expression (Fig. 3f), which was intriguing given this tissue's mass, strong physical activation during restraint stress, and abundant production of cytokines and chemokines[28,29]. The increase in *Cxcl1* mRNA in the muscle was very rapid (Fig. 3g and Extended Data Fig. 4i), and was closely followed by an increase in muscle CXCL1 protein, arguing for de novo synthesis (Fig. 3h). However, muscle *Cxcl1* mRNA, serum CXCL1 protein and blood neutrophils

did not increase in response to voluntary running (Fig. 3i and Extended Data Fig. 4j), suggesting that very strong muscle activation, as confirmed by electromyography telemetry, was required (Extended Data Fig. 4k and Extended Data Fig. 4l). Circulating markers of muscle damage were not elevated after restraint stress suggesting that no major muscle injury had occurred (Extended Data Fig. 4m).

Next, we sought to identify what controls muscle CXCL1 production during acute stress. We found that spinal cord transection eliminated CXCL1 in the paralysed skeletal muscle and prevented blood neutrophilia (Fig. 3j), indicating that the brain's signals are conveyed through neuronal pathways in the spinal cord. To determine whether motor innervation of the muscle itself was responsible for CXCL1 augmentation, we targeted the neuromuscular junction as the most downstream site using low doses of the non-depolarizing muscle relaxant rocuronium. At the dose used, rocuronium induced general muscle weakness and prevented excessive movement but did not interfere with normal respiration. This intervention blunted the stress-induced increase in muscle *Cxcl1* and blood neutrophils (Fig. 3k), suggesting that central motor circuits control stress-induced neutrophilia.

To test the role of central motor circuits directly, we implemented optogenetics. Stimulating forelimb-related motor areas in the right motor cortex of Thy1-ChR2-YFP mice[30,31] amplified *Cxcl1* mRNA in the left but not right biceps (Fig. 3l). The increase in *Cxcl1* was small, which was expected given the low strength of muscle movement induced by optogenetic stimulation under anaesthesia. To induce stronger muscle movement, we optogenetically targeted motor centres in the medulla, where many motor circuits converge[32] (Extended Data Fig. 4n,o), leading to widespread skeletal muscle movement and strongly raising *Cxcl1* mRNA in various skeletal muscles (Fig. 3m). Correspondingly, we found elevated CXCL1 in the serum, along with blood neutrophilia (Fig. 3m).

Having demonstrated that stimulation of central motor structures induces CXCL1 and neutrophilia, we wondered whether inhibiting these structures during restraint stress prevents neutrophilia. First, bilaterally ablating the motor cortex (Extended Data Fig. 4p) slightly impaired muscle movement[33] and blunted restraint stress-induced neutrophilia (Fig. 3n). Second, chemogenetically inhibiting glutamatergic neurons in the rostral medulla (Extended Data Fig. 4q) inhibited movement and prevented restraint-induced neutrophilia (Fig. 3o). By combining optogenetics with muscle relaxation, we found that optogenetic medulla stimulation in the presence of a peripheral muscle relaxant no longer induced neutrophilia (Fig. 3p). Thus, neutrophilia arises as a consequence of central motor circuit-controlled excessive muscle activity.

Effects of stress on innate immunity

Leukocytes communicate across organ systems, relying on specialized tissues for immune surveillance. Our data show that the leukocyte tissue landscape adapts rapidly to acute stress. First, acute stress mobilizes substantial numbers of neutrophils to the blood and, from there, they can infiltrate peripheral organs, presumably participating in inflammation. Second, acute stress prevents lymphocytes, albeit temporarily, from occupying lymph nodes and therefore from surveying antigens on antigen-presenting cells, potentially limiting adaptive

immunity. Given such widespread and sweeping relocations, we examined how leukocyte tissue distribution and function influence disease.

We started with bulk RNA-sequencing (RNA-seq) analysis of blood neutrophils sorted under various stress conditions (Extended Data Fig. 5a). Principal component analysis revealed distinct clustering among the groups (Extended Data Fig. 5b); the strongest expression differences in important neutrophil-function-related genes appeared after 1 h of stress (Extended Data Fig. 5c), with diminishing differences between non-stressed and recovering animals (Extended Data Fig. 5d). Hierarchical clustering showed transcripts that changed in both directions after 1 h of stress and that either returned to pre-stress levels or remained altered even after 3 h of recovery (Extended Data Fig. 5e). Crucial immunological pathways were enriched after stress (Extended Data Fig. 5f).

To examine stress-induced changes among neutrophil subsets, we performed single-cell RNA-seq (scRNA-seq) analysis. We noted at least four neutrophil clusters (Extended Data Fig. 5g), some of which changed in response to stress (Extended Data Fig. 5h). Among them, a cluster defined by neutrophil degranulation, activation and aggregation expanded in response to stress (Extended Data Fig. 5i). Some of these clusters resembled those described in a recent single-cell analysis of neutrophil heterogeneity in the blood[34] (Extended Data Fig. 5j). Moreover, we noted that stress accelerates neutrophil maturation (Extended Data Fig. 5k) according to a neutrophil maturation score[34,35]. Comparing key neutrophil mediators (Extended Data Fig. 5l) further bolstered the idea that acute stress elevates the ability of neutrophils to modulate inflammation. Indeed, we observed that neutrophils readily accumulated at sites of injury (Extended Data Fig. 5m), consistent with previous findings[36]. CXCL1 injection alone recapitulated only a small fraction of the neutrophil gene expression changes that were otherwise observed during restraint stress (Extended Data Fig. 5n), suggesting that CXCL1 recruits neutrophils out of the bone marrow (Extended Data Fig. 4h) as previously described[25,26], but additional cues are responsible for their functional changes.

Effects of stress on autoimmunity

To assess the potential implications of stress-induced leukocyte redistribution from the lymph nodes to the bone marrow, we used models of autoimmunity and viral infection. Although the substantial reduction in the number of adaptive immune cells in the lymph nodes during acute stress might appear to be detrimental, restricting the acquisition of adaptive immunity may be beneficial under certain conditions. We began testing these ideas by subjecting mice to experimental autoimmune encephalomyelitis (EAE)[37] (Fig. 4a). Consistent with earlier data, we found fewer B and T cells in the lymph nodes of EAE mice that were exposed to stress (Fig. 4b) but more B and T cells in the bone marrow (Fig. 4c). We enumerated leukocytes in the spinal cord and found considerably less inflammation in mice that were stressed during sensitization (Fig. 4d). As a consequence, mice that were subjected to stress had lower EAE clinical scores (Fig. 4e) and were protected from disease initiation and progression.

To link the influence of stress on the acquisition of autoimmunity to relevant brain regions, we applied chemogenetics. We stimulated CRH neurons in the PVH during the induction phase of EAE and found less severe disease initiation compared with the controls (Fig. 4f). Conversely, we tested the effect of stress on EAE initiation in mice that genetically lacked CRH in the hypothalamus, and found that the protective effect of stress on acquisition of EAE was abrogated (Fig. 4g). Compared with the control mice, mice lacking hypothalamic CRH were highly susceptible to EAE even when stressed (Fig. 4g). These data show that stress activates specific brain regions that prevent the acquisition of autoimmunity.

Effects of stress on viral infection

To test how lymphocyte redistribution from the lymph nodes to the bone marrow affects immunity to viral infections, we infected K18-hACE2 mice with SARS-CoV-2 (ref.[38]), and exposed them to episodes of acute restraint stress (Fig. 5a). We observed fewer B cells and T cells in the lung-draining mediastinal lymph nodes on day 7 (Fig. 5b). Compared with the control mice, the stressed mice had higher viral titres (Fig. 5c) and died at higher rates from SARS-CoV-2 infection (Fig. 5d). Second, we infected mice with influenza A virus (IAV) (Fig. 5e). Similar to the observations generated using SARS-CoV-2, we found that stressed mice had smaller mediastinal lymph nodes (Fig. 5f), containing fewer lymphocytes (Fig. 5g,h). Stressed mice also had fewer IAV-specific antibodies in the bronchoalveolar lavage[39] (BAL) (Fig. 5i), which resulted in higher lung viral loads (Fig. 5j) and more severe pathology (Fig. 5k). These data suggest that acute stress during the early phase of virus exposure impairs host adaptive immunity against infections.

To connect the effects of stress on the acquisition of adaptive antiviral immunity with the relevant brain regions, responsive cell types and receptors, we applied chemogenetic approaches as well as various knockout models in the context of IAV infection. We found that selective stimulation of PVH CRH neurons recapitulated the long-lasting effect of stress on lymphocyte numbers in mediastinal lymph nodes (Fig. 5g,h), IAV-specific antibody titres in the BAL (Fig. 5i) and pulmonary viral loads (Fig. 5j), whereas selective ablation of PVH CRH neurons prevented the detrimental effect of stress on these parameters. We also examined the relevant immune cells and receptors and observed no effect of stress on viral loads in *Rag1*-KO, *Tcra*-KO and muMT mice (Extended Data Fig. 6). We infected $Cd19^{cre+/-};Nr3c1^{flox+/+}$ and $Cd4^{cre+/-};Nr3c1^{flox+/+}$ (B- and T-cell specific *GR*-KO, respectively) mice and observed no stress-induced changes in the number of the respective cell type in the mediastinal lymph nodes (Fig. 5g,h); mice lacking the GR on B cells exhibited no stress-induced decrease in the IAV-specific antibody titres in the BAL (Fig. 5i) and neither *GR*-KO line showed stress-induced increases in pulmonary viral loads (Fig. 5j). Although CRH-neuron-mediated lymphocyte reduction in lymph nodes is important in impairing the body's ability to fight viral infections, other glucocorticoid effects probably also contribute[40]. These data reveal a pathway that links stress-induced PVH CRH neuron activity to corticosterone acting directly on lymphocytes, therefore impairing sensitization to viral infection and aggravating disease.

Leukocytes are motile cells that perform immune surveillance and shape the course of immunity and inflammation. The physiological adaptation to acute stress not only elicits

fight or flight but can also modulate the organism's response to looming injury or infection. Our study reveals how specific neuron clusters located in diverse regions of the brain relevant to fear and the fight or flight response cause massive changes in leukocyte distribution and function (Extended Data Fig. 7). Future studies are required to deepen our understanding of these neuroimmune pathways.

Methods

Animals

Wild-type (C57BL/6J), C57BL/6-Tg(UBC-GFP)30Scha/J (UBI-GFP[+]), B6.129P2(C)-Cd19[tm1(cre)Cgn]/J (CD19-Cre), B6.Cg-Tg(Cd4-cre)1Cwi/BfluJ (CD4-Cre), B6.129P2-Lyz2[tm1(cre)Ifo]/J (LysM-Cre), B6.Cg-Nr3c1[tm1.1Jda]/J (GR[flox]), B6(Cg)-Crh[tm1(cre)Zjh]/J (CRH-ires-Cre), B6.FVB(129X1)-Tg(Sim1-cre)1Lowl/J (Sim1-Cre), B6.129S4(Cg)-Crh[tm2.1Maj]/J (CRH[flox]), B6J.129S6(FVB)-Slc17a6[tm2(cre)Lowl]/MwarJ (Vglut2-ires-Cre), B6J.B6N(Cg)-Cx3cr1[tm1.1(cre)Jung]/J (Cx3cr1-Cre), B6.129X1-Gt(ROSA)26Sor[tm1(EYFP)Cos]/J (R26-stop-EYFP), B6.Cg-Tg(Thy1-COP4/EYFP)18Gfng/J (Thy1-ChR2-YFP), Adrb1[tm1Bkk] Adrb2[tm1Bkk]/J (*Adrb1^{−/−};Adrb2^{−/−}*), B6.129S2-*Il6[tm1Kopf]*/J (*Il6^{−/−}*),B6.Cg-Tg(K18-ACE2)2Prlmn/J (K18-hACE2), B6.129S7-Rag1[tm1Mom]/J (*Rag1*-KO), B6.129S2-Tcra[tm1Mom]/J (*Tcra*-KO) and B6.129S2-Ighm[tm1Cgn]/J (muMt) mice were purchased from The Jackson Laboratory. B6.FVB(Cg)-Tg(Dbh-cre)KH212Gsat/Mmucd (DBH-Cre) were purchased from the MMRRC at the University of California Davis. *Adrb2^{−/−};Adrb3^{−/−}* mice were provided by P.S.F. Genotyping for each strain was performed as recommended on the Jackson Laboratory website. Relevant mice were crossed to generate *Cd19[cre+/−];Nr3c1[flox+/+]*; *Cd4[cre+/−];Nr3c1[flox+/+]*; *LysM[cre+/−];Nr3c1[flox+/+]*; *Cx3cr1[cre+/−];Nr3c1[flox+/+]* plus respective *Nr3c1[flox+/+]* controls, as well as *Sim1[cre+/−];Crh[flox+/+]* plus respective *Crh[flox+/+]* controls. *Cd19[cre+/−];EYFP^{+/−}*; *Cd4[cre+/−];EYFP^{+/−}*, *LysM[cre+/−];EYFP^{+/−}* and Cx3cr1-Cre^{+/−}:EYFP^{+/−} were generated as reporter mice. All experiments were performed on mice aged 6 weeks to 6 months with age- and sex-matched controls. All mice were housed on a 12 h–12 h light–dark cycle at 22 °C with a humidity range of 30–70% and unrestricted access to food and water. During stress experiments and after surgery, mice were singly housed. Where appropriate, mice were randomly assigned to groups and experiments were performed in a blinded manner. All protocols were approved by the Animal Review Committee at the Massachusetts General Hospital (protocols 2011N000035 and 2015N000044) and/or the Animal Review Committee at the Mount Sinai Hospital (PROTO202000262 and IPROTO202200000035) and complied with all relevant ethical regulations.

In vivo interventions and procedures

Stress models.—Mice were single-housed and habituated to the environment before any stress interventions. New environmental stress was introduced by placing mice into clean, new cages. Predator odour stress was induced by placing a tissue soaked with 0.5 ml of bobcat urine into the home cages of the mice. Social intruder stress was created by placing an aggressive male mouse into the home cage of the experimental mouse. Restraint stress was generated by placing mice into well-ventilated conventional restraint cylinders without

squeezing. Different stress and recovery durations as well as frequencies were used as indicated.

Intravital microscopy.—Non-stressed mice versus mice restraint-stressed for 1 h for neutrophil imaging, as well as non-stressed mouse versus mice restraint-stressed for 4 h for B cell, T cell and monocyte imaging, were anaesthetized with 1–3% isoflurane and 2 l min^{-1} oxygen anaesthesia. Mice were kept on a 37 °C heating plate during the whole procedure. The fluorescence agents FITC-dextran (2×10^6 Da) for labelling the vasculature and PE-labelled antibodies to visualize different cell types (5 μl antibody stock in 50 μl PBS) were injected intravenously and one mouse ear was immobilized on a 37 °C heated aluminium plate for confocal imaging. Without delay, the mice were imaged under isoflurane anaesthesia. The whole imaging procedure was kept to a maximum of 1 h. Imaging was performed using an Olympus XLUMPLFLN 20X W NA:1.00 water-immersion objective on an Olympus custom made confocal multi-photon microscope using 473 nm and 559 nm diode-lasers with a DM405/473/559 dichroic mirror, a SDM560 beam splitter, and BA490–540 and BA575–675 emission filters (Olympus). Neutrophils were labelled using PE-labelled anti-Ly-6G antibodies; B cells with PE-labelled anti-CD19 antibodies; T cells with PE-labelled anti-CD3 antibodies; and monocytes with PE-labelled anti-CD115 antibodies.

GFP$^+$ bone marrow transfer.—GFP$^+$ bone marrow cells were collected from femurs and tibias of UBI-GFP$^+$ donor mice, processed for red blood cell lysis and intravenously injected into naive C57BL/6J mice (~25×10^6 GFP$^+$ bone marrow leukocytes per recipient). Mice were allowed to recover for 8 h before stress interventions.

GFP$^+$ peripheral leukocyte transfer.—GFP$^+$ leukocytes were collected from the blood and spleen of UBI-GFP$^+$ donor mice, processed for red blood cell lysis and intravenously injected into naive C57BL/6J mice (42×10^6 GFP$^+$ leukocytes per recipient (Fig. 1e); 18×10^6 GFP$^+$ leukocytes per recipient (Fig. 1f)). Mice were allowed to recover before stress interventions (for 12 h in the experiment presented in Fig. 1e and 10 h in the experiment presented in Fig. 1f).

Catecholamine injections.—Non-stressed C57BL/6J mice were intraperitoneally injected with either vehicle (saline) or noradrenaline (0.2 μg kg^{-1}–2,000 μg kg^{-1}, Sigma-Aldrich) under short isoflurane anaesthesia. Blood was withdrawn and analysed 1 h after injection.

Corticosterone injections.—Non-stressed C57BL/6J mice were intraperitoneally injected with either vehicle (saline) or corticosterone (5 mg kg^{-1}, Corticosterone: HBC complex, Sigma-Aldrich) under short isoflurane anaesthesia. Blood was withdrawn and analysed 1 h and 4 h after injection.

AMD3100 injections.—Non-stressed C57BL/6J mice were intraperitoneally injected with either vehicle (PBS) or AMD3100 (10 mg kg^{-1}, AMD3100 octahydrochloride, Abcam) under short isoflurane anaesthesia. After 30 min, half of the mice from each treatment group were stressed, and the other half remained non-stressed. Blood was withdrawn 4 h later.

Sympathectomy.—Chemical sympathectomy was induced by three intraperitoneal injections of 6-hydroxydopamine hydrobromide (6-OHDA in 0.1% sodium metabisulfite in 0.9% sterile saline, total of 3×5 mg per mouse, injections 3 days apart, Sigma-Aldrich) under short isoflurane anaesthesia. Mice injected with 0.1% sodium metabisulfite in 0.9% sterile saline served as vehicle-treated controls.

α- and β-adrenergic receptor blockade.—Non-stressed C57BL/6J mice were intraperitoneally injected with either vehicle (saline) or propranolol (30 mg kg^{-1}, propranolol hydrochloride, Sigma-Aldrich) and phentolamine (30 mg kg^{-1}, phentolamine hydrochloride, Sigma-Aldrich) under short isoflurane anaesthesia. Then, 75 min after injection, baseline blood was withdrawn under short isoflurane anaesthesia. After a short recovery from the isoflurane, the mice were restraint-stressed for 20 min and then allowed to recover for 40 min before blood was withdrawn again.

AZD5069 injections.—Non-stressed C57BL/6J mice were intraperitoneally injected with either vehicle (25% DMSO, 75% corn oil) or AZD5069 (100 mg kg^{-1}, Selleck Chemicals) under short isoflurane anaesthesia. After 30 min, half of the mice from each treatment group were restraint-stressed for 1 h, and the other half remained non-stressed. Blood was withdrawn immediately after 1 h restraint stress.

CXCL1 injections.—Non-stressed C57BL/6J mice were intraperitoneally injected with either vehicle (PBS) or CXCL1 (50 ng or 500 ng per mouse as indicated, recombinant mouse CXCL1/KC protein, R&D Systems) under short isoflurane anaesthesia. After 1 h, blood was drawn for flow analyses or for fluorescence-activated cell sorting (FACS) analysis of blood neutrophils.

Muscle relaxation.—To specifically block motor impulse transmission from the lower motor neurons' axon terminals to the skeletal muscles, we intravenously injected a low dose of the non-depolarizing muscle relaxant rocuronium (0.05 mg kg^{-1}). As in previous reports, this very low dose of rocuronium did not interfere with normal breathing[41] and only induced muscle weakness and prevented the excessive muscle activity that normally occurs during restraint stress. Specifically, non-stressed WT mice were intravenously injected with either vehicle (PBS) or rocuronium (0.05 mg kg^{-1}, rocuronium bromide, Sigma-Aldrich) under brief isoflurane anaesthesia. After a short recovery from the anaesthesia, half of the mice from each treatment group were restraint-stressed for 3 min, and the other half remained non-stressed. Blood and organs were collected 15 min after the restraint stress episode. The same dose was used to induce muscle relaxation during optogenetic medulla stimulation as outlined below.

Voluntary exercise.—Mice had free access to a low-profile wireless running wheel (ENV-047; Med Associates) in their home cage. Wheels were wirelessly connected to a USB Hub and a computer with analyses software (Med Associates).

EAE.—EAE induction and clinical scoring were performed according to the manufacturer's instructions (Hooke Laboratories, kit EK-2110). In brief, mice were injected subcutaneously with the antigen MOG$_{35-55}$ in emulsion with complete Freund's adjuvant (CFA). Then, 1

h and 24 h later, the mice were intraperitoneally injected with 100 ng of pertussis toxin (PTX). Clinical scores were determined daily until day 28 after disease induction. Mice were euthanized at the indicated timepoints. To evaluate the effect of psychological stress on EAE induction, mice were restraint-stressed for 4 h immediately before MOG_{35-55}/CFA injection on day 0, for 4 h directly before the second PTX injection on day 1 and subsequently for 4 h once daily until day 9 (a total of ten 4 h episodes). Control mice were not exposed to restraint stress. To determine the effect of chemogenetic stimulation of hypothalamic CRH neurons on EAE induction, Crh^{cre} mice that had received the activating pAAV-hSyn-DIO-hM3D(Gq)-mCherry into their PVH 3 weeks earlier were intraperitoneally injected with clozapine-*N*-oxide (CNO, 5 mg kg^{-1}, clozapine-*N*-oxide hydrochloride, Sigma-Aldrich) 4 h before MOG_{35-55}/CFA injection on day 0, 4 h before the second PTX injection on day 1 and then once daily until day 9 (a total of ten CNO injections). Control mice received corresponding saline injections.

Surgical interventions

Adrenalectomy.—Both adrenal glands were surgically removed through bilateral dorsolateral subcostal access routes. Sham-operated mice were used as controls. After surgery, adrenalectomized mice received saline as drinking water. Mice were allowed to recover for >7 days before further manipulation.

Splenectomy.—The spleen was surgically removed through a small anterolateral subcostal incision. Sham-operated mice were used as controls. Mice were allowed to recover for >7 days before further manipulation.

Spinal cord transection.—Spinal cord transections were performed through a laminectomy at the lower thoracic level. Sham-operated mice were used as controls. Stress experiments were conducted on the first post-operative day to prevent muscle atrophy and other mid- and long-term complications of spinal cord transection.

EMG telemetry implantation.—To record the electric signals from skeletal muscle under relaxed conditions, during voluntary running and during restrain stress, WT mice were implanted with EMG telemetry devices (HD-X02, Data Science International). The device was implanted subcutaneously with the electrodes fixed in the gluteal and upper leg musculature. The wirelessly received data were analysed using the Neuroscore software (DSI). Each mouse was recorded under each condition on subsequent days during their active period, data were expressed as the number of amplitude peaks above a mouse-specific threshold of 0.2 mV (2 mice) or 0.4 mV (1 mouse) during the first 10 min of restraint.

Subcutaneous sponge implantation.—WT mice were either restraint-stressed or remained non-stressed for 2 h directly before subcutaneous implantation of a small sterile gelatin sponge (Gelfoam, Pfizer) on their back. Neutrophil recruitment into the sponge was quantified by flow cytometry 18 h after sponge implantation.

Stereotactic surgery.—In brief, mice were anaesthetized with isoflurane and buprenorphine was administered subcutaneously. Body temperature was maintained by a

heating pad. The mouse head was placed into the stereotactic frame (Stoelting; ultra precise specialized mouse stereotaxic instrument with mouse anaesthesia mask). After sagittal midline incision, the skull with the bone sutures was exposed and horizontal placement was achieved by adjusting bregma (intersection of coronal and sagittal suture) and lambda (intersection of lambdoid and sagittal suture) to the same height. Coordinates for trepanation were determined using a mouse brain atlas (Paxinos) and a small hole was drilled above the target area. Subsequently, a Hamilton syringe was advanced to the respective depth and the virus solution was administered. The needle was left in place for 2–10 min and subsequently slowly withdrawn. In optogenetic experiments, a cannula was implanted 200 μm above the virus injection site and fixed to the skull with dental cement. The wound was closed with sutures and mice were housed individually.

Chemogenetics.—For chemogenetic stimulation of CRH neurons in the PVH, Crh^{cre} mice received two injections of a viral vector encoding Cre-dependent expression of the DREADD receptor hM3D(Gq)-mCherry, or a control viral vector encoding Cre-dependent expression of mCherry only, into the PVH (bregma coordinates: −0.4 mm and −0.9 mm AP, −0.4 mm ML, −5.0 mm DV; 1 μl each). pAAV-hSyn-DIO-hM3D(Gq)-mCherry was a gift from B. Roth (Addgene viral prep, 44361-AAV2); pAAV-hSyn-DIO-mCherry was a gift from B. Roth (Addgene viral prep, 50459-AAV2). Animals were allowed to recover from surgery for 3 weeks before intraperitoneal injections of CNO (5 mg kg^{-1}) under short isoflurane anaesthesia. Control mice received saline injections. Blood was withdrawn for analyses 4 h or 5 h after CNO injection as indicated.

To ablate CRH neurons in the PVH, Crh^{cre} mice received two bilateral injections of a viral vector encoding Cre-dependent expression of Caspase-3 into the PVH (bregma coordinates: −0.4 mm and −0.9 mm AP, ±0.4 mm ML, −5.0 mm DV; 1 μl each). Control mice received injections of the control virus pAAV-hSyn-DIO-mCherry at the same coordinates and volumes. AAV-flex-taCasp3-TEVp was a gift from N. Shah (UNC Vector Core). pAAV-hSyn-DIO-mCherry was a gift from B. Roth (Addgene viral prep, 50459-AAV2). Four weeks after surgery, mice were restraint-stressed for 4 h and blood was withdrawn at the baseline and directly after the stress episode.

For chemogenetic inhibition of glutamatergic neurons in the medulla, vGlut2^{Cre} mice received bilateral injections of a viral vector encoding Cre-dependent expression of the DREADD receptor hM4D(Gi)-mCherry into the medulla (bregma coordinates: −6.6 mm AP, ±1.25 mm ML, −4.32 mm DV; 1.0 μl each). pAAV-hSyn-DIO-hM4D(Gi)-mCherry was a gift from B. Roth (Addgene viral prep, 44362-AAV2). Animals were allowed to recover from surgery for >3 weeks before they received intraperitoneal injections of CNO (two injections 20 min apart, total of 10 mg kg^{-1}) or saline under short isoflurane anaesthesia. Mice were exposed to 30 min of restraint stress starting 15 min after the second CNO/saline injection and blood was withdrawn for analyses immediately after stress cessation.

Optogenetics.—For optogenetic stimulation of catecholaminergic neurons in the rostroventrolateral medulla (RVLM), Dbh^{cre} mice received one unilateral injection of a viral vector encoding Cre-dependent expression of the light-sensitive humanized channelrhodopsin H134R mutant hChR2(H134R) into the RVLM (bregma coordinates:

−6.68 mm AP, −1.2 mm ML, −4.8 mm DV; 1 μl). A fibre optic cannula (200 μm, 0.39 NA, Thorlabs, CFML12L05) was implanted 300 μm above the injection site. Animals were allowed to recover from surgery for 3 weeks before being connected to the fibre optic patch cable (Thorlabs, M89L01). To activate RVLM neurons expressing hChR2(H134R), 10 ms light pulses from a 470 nm fibre-coupled LED (Thorlabs, M470F3) were delivered at a frequency of 20 Hz for a total duration of 5 min. Using a power meter (Thorlabs, PM20A), light intensity was adjusted to 5 mW at the end of the fibre optic cannula. hChR2(H134R)-injected Dbh^{cre} mice attached to the fibre optic patch cable but without light stimulation were used as controls. Blood was withdrawn for analyses 1 h after the onset of stimulation. pAAV-EF1a-double floxed-hChR2(H134R)-mCherry-WPRE-HGHpA was a gift from K. Deisseroth (Addgene viral prep, 20297-AAV1). Experiments were conducted in two rounds with a cross-over design in which each mouse was analysed once with and once without LED stimulation 1 day apart, for a total of $n = 8$ per group.

To optogenetically stimulate glutamatergic neurons in the medulla, vGlut2^{Cre} mice received one unilateral injection of a viral vector encoding Cre-dependent expression of the light-sensitive humanized channelrhodopsin H134R mutant hChR2(H134R) into the medulla (bregma coordinates: −6.6 mm AP, −1.25 mm ML, −4.32 mm DV; 0.5 μl). A fibre optic cannula (200 μm, 0.39 NA, Thorlabs, CFML12L05) was implanted 200 μm above the injection site. Animals were allowed to recover from surgery for 2 weeks before being connected to the fibre optic patch cable (Thorlabs, M89L01). To activate excitatory neurons expressing hChR2(H134R) in the medulla, 10 ms light pulses from a 470 nm fibre-coupled LED (Thorlabs, M470F3) were delivered at a frequency of 20 Hz with the following pattern: 3 min stimulation on, 2 min stimulation off, over a total period of 30 min. Using a power meter (Thorlabs, PM20A), light intensity was adjusted to 5 mW at the end of the fibre optic cannula. hChR2(H134R)-injected vGlut2^{Cre} mice attached to the fibre optic patch cable but without light stimulation were used as controls. Blood and tissues were collected for analyses at the end of the stimulation period. pAAV-EF1a-double floxed-hChR2(H134R)-mCherry-WPRE-HGHpA was a gift from K. Deisseroth (Addgene viral prep, 20297-AAV1).

To test the effect of peripheral muscle relaxation during optogenetic medulla stimulation on neutrophilia, we used the same experimental approach, except for a shorter stimulation duration of only 3 min (with otherwise the same stimulation parameters) directly after injection of the muscle relaxant rocuronium or vehicle (PBS) under brief isoflurane anaesthesia as described above. The animals were allowed to recover for 27 min after the end of the stimulation period before samples were taken. The shorter stimulation duration was necessary owing to the short half-life of rocuronium at the low dose administered. In a cross-over design, the experiment was repeated with changed groups 2 days later.

To stimulate channelrhodopsin-expressing neurons in the right hemispheric motor cortex of Thy1-ChR2-YFP mice, we first removed a portion of skull to expose the entire right hemispheric motor cortex, under isoflurane anaesthesia. At this point, anaesthesia was changed to ketamine/xylazine and the motor area was test-stimulated with a fibre optic cannula (200 μm, 0.39 NA, Thorlabs, CFML12L05) connected to a fibre optic patch cable (Thorlabs, M89L01) and a 470 nm fibre-coupled LED (Thorlabs, M470F3). The cannula

delivering 5 ms pulses at a frequency of 20 Hz with 5 mW output power measured at the tip of the cannula (1 s stimulation on–1 s stimulation off) was moved across the entire motor area between (+2.0 mm to −2.0 mm AP and 0.0 mm to −2.5 mm ML) to identify the spot that induced the strongest motor response of the contralateral front limb. This spot was then stimulated for 30 min with the same parameters as during the screening phase (20 Hz, 5 ms pulse duration, 5 mW output power, 1 s stimulation on–1 s stimulation off). The dura remained intact during the whole procedure and a droplet of corn oil was applied to the area to facilitate light penetration. After the stimulation period, blood and organs were collected for analyses. Control mice underwent the same procedures but without any light stimulation.

Vacuum suction was used to bilaterally ablate the motor cortex of WT mice between the following bregma coordinates: +2.5 mm to −2.0 mm AP, ±0.5 mm to ±2.75 mm ML, −0.75 mm DV. Sham mice underwent the same stereotactic procedure including skull removal but without vacuum ablation. After recovery, mice were restraint-stressed for 1 h or remained non-stressed and blood was withdrawn directly after the stress episode.

Viral infection models

IAV.—C57BL/6J mice, $Rag1$-KO mice, $Trca$-KO mice, muMT mice, PVH CRH-neuron-ablated mice (Cre-dependent Caspase-3 encoding AAV in the PVH of Crh^{cre} mice), B-cell-specific $Nr3c1$-KO mice ($Cd19^{cre+/−}$;$Nr3c1^{flox+/+}$ mice), and T-cell-specific $Nr3c1$-KO mice ($Cd4^{cre+/−}$;$Nr3c1^{flox+/+}$ mice) were either restraint-stressed for 4 h (stressed group) or remained non-stressed (non-stressed group). Subsequently, both groups were anaesthetized using isoflurane and intranasally infected (in 25 μl) with a sublethal dose (50 or 35 plaque-forming units (PFU)) of the IAV strain influenza A/Puerto Rico/8/34 (H1N1). Sublethal doses were determined for each passage and were determined to be 50 PFU and then 35 PFU. On day 1 and 2 after infection, mice in the stressed group were again subjected to 4 h of restraint stress for a total of three restraint-stress episodes. Afterwards, the mice remained in their home cages under non-stressed conditions until they were euthanized on day 9 after infection for analyses. Viral titres were determined in lung homogenates (homogenized in 500 μl PBS) using standard Madin–Darby canine kidney cell (MDCK) plaque assays.

Non-stressed Crh^{cre} mice with hM3D(Gq) in the PVH were injected with CNO (stimulated group) or saline (control group) as described above 4 h before IAV infection. Subsequently, both groups were anaesthetized using isoflurane and intranasally infected (in 25 μl) with a sublethal dose (50 PFU) of the IAV strain influenza A/Puerto Rico/8/34 (H1N1). On day 1 and 2 after infection, mice received another 2 injections of CNO (stimulated group) or saline (control group) per day (D0: 1 × CNO/ saline; D1 + D2: 2 × CNO/saline per day). Afterwards, mice remained in their home cages under non-stressed conditions until they were euthanized on day 9 after infection for analyses. Viral titres were determined in lung homogenates (homogenized in 500 μl PBS) using standard MDCK plaque assays.

SARS-CoV-2 infection.—K18-hACE2 mice were either restraint-stressed for 4 h (stressed group) or remained relaxed (relaxed group). Immediately after the initial stress episode, all mice were anaesthetized by isoflurane and infected intratracheally (in 40 μl) with SARS-CoV-2 (strain SB2; provided by S. Mubareka) at a dose of 3,000 PFU. On

days 1 and 2 after infection, the mice in the stressed group were again subjected to 4 h of restraint stress for a total of three restraint-stress episodes. The mice were then returned to their home cages under relaxed conditions until they were euthanized on day 7 for further analyses (Fig. 5b–d) or when they became moribund (survival experiments in Fig. 5e). Viral titres were determined in lung homogenates (homogenized in 500 µl PBS) using Vero cell Reed–Muench median tissue culture infectious dose assays.

Cells

Cell lines and culture.—IAV viral quantification was performed by MDCK plaque assay. Cells were obtained from the American Type Culture Collection (ATCC) and maintained in Dulbecco's modified Eagle medium (DMEM) enriched with 10% (v/v) heat-inactivated FBS, 2 mM L-glutamine and 100 U ml^{-1} penicillin–streptomycin. Vero cells were obtained from the ATCC and maintained in DMEM enriched with 10% (v/v) heat-inactivated FBS and 100 U ml^{-1} penicillin–streptomycin.

Cell collection.—Blood was collected and RBC lysis buffer (BioLegend) was used twice to lyse the red blood cells. After transcardiac perfusion with PBS (Thermo Fisher Scientific), organs (lung, liver, muscle, skin, aorta and spinal cord) were collected, minced and digested in a mixture of 450 U ml^{-1} collagenase I, 125 U ml^{-1} collagenase XI, 60 U ml^{-1} DNase and 60 U ml^{-1} hyaluronidase (Sigma-Aldrich) in PBS for 20 min (liver), 30 min (spinal cord), 40 min (lung, muscle, aorta) or 60 min (lung and skin) on a shaker (at 800 rpm) at 37 °C. Next, the digested organ was flushed through a 40 µm cell strainer. Spinal cord suspensions were further purified using a Percoll density gradient (30% upper and 70% lower phase). The cell layer between the two phases was collected and washed in PBS. Spleens were pressed through a 40 µm cell strainer and RBC lysis buffer was used to lyse the red blood cells. Lymph nodes were pressed through a 40 µm cell strainer. Bone marrow cells were flushed from the bone marrow cavities and brought into a single-cell suspension by pipetting up and down; then, RBC lysis buffer was used to lyse the red blood cells.

Cell sorting.—After cell surface marker staining, the indicated cell populations were sorted on a FACS Aria II sorter (BD Biosciences) directly into collection medium or empty tubes.

Flow cytometry.—Single-cell suspensions were stained in FACS buffer (0.5% BSA and 2 mM EDTA in PBS) containing fluorophore-coupled antibodies at a concentration of 1:700 at 4 °C for 15 min, unless otherwise indicated. To differentiate between live and dead cells, the cell suspensions were stained with Zombie Aqua (BioLegend) at a concentration of 1:1,000 in PBS at 4 °C for 15 min or by adding propidium iodide directly before flow cytometry analyses. The following antibodies were used for flow cytometry: anti-Ly-6G (BioLegend, 1A8), anti-NK1.1 (BioLegend, PK136), anti-CD19 (BioLegend, 6D5), anti-CD90.2 (BioLegend, 30-H12), anti-CD3 (BioLegend, 17A2), anti-CX3CR1 (BioLegend, 5A011F11), anti-CD45 (BioLegend, 30-F11), anti-CD4 (BioLegend, GK1.5), anti-CD62L (BioLegend, MEL-14), anti-B220 (BioLegend, RA3–6B2), anti-Ly-6C (BioLegend, HK1.4), anti-CD11b (BioLegend, M1/70), anti-CD8 (BioLegend, 53–6.7), anti-MHCII (BioLegend, M5/114.15.2), anti-F4/80 (BioLegend,

BM8), anti-IgD (BioLegend, 11–26c.2a), anti-CD24 (BioLegend, M1/69), anti-IgM (BioLegend, RMM-1), anti-CD93 (BioLegend, AA4.1), anti-CD43 (BioLegend, 1B11), anti-CD115 (BioLegend, AFS98), anti-CD34 (eBioscience, RAM34), anti-CD135 (BioLegend, A2F10), anti-KIT (BioLegend, 2B8), anti-Sca-1 (BioLegend, E13–161.7), anti-CD11c (BioLegend, N418), anti-CD48 (BioLegend, HM48–1), anti-CD16/32 (BioLegend, 93), anti-CD150 (BioLegend, TC15–12F12.2), anti-CD49b (BioLegend, DX5), anti-Ter119 (BioLegend, TER-119), anti-IL-7Ra (BioLegend, SB/199), anti-Siglec-F (BioLegend, S17007L), anti-FcεRIα (BioLegend, MAR-1), anti-BrdU (eBioscience, BU20A). Influenza-specific CD8$^+$ T cells were identified with NP (ASNENMETM)-loaded H-2Db tetramers conjugated to APC (1:600 dilution; National Institutes of Health Tetramer Core Facility, Emory University Vaccine Center). Cells were identified as: (1) B cells (CD45$^+$ B220$^+$CD19$^+$CD11b$^-$), (2) CD4 T cells (CD45$^+$CD3$^+$CD90.2$^+$CD4$^+$CD11b$^-$), (3) CD8 T cells (CD45$^+$CD3$^+$CD90.2$^+$CD8$^+$CD11b$^-$), (4) Ly-6C^{high} monocytes (CD45$^+$Lin1$^-$CD11b$^+$CX3CR1$^+$CD115$^+$F4/80$^-$Ly-6C^{high}), (5) neutrophils (CD45$^+$Lin1$^-$CD11b$^+$Ly-6G$^+$F4/80$^-$), (6) macrophages (CD45$^+$Lin1$^-$CD11b$^+$F4/80$^+$Ly-6C^{low}), (7) eosinophils (CD45$^+$SSC^{high}CD11b$^+$Ly-6G$^-$Siglec-F$^+$), (8) basophils (CD45$^+$CD11b$^+$Ly-6G$^-$Fcε(RI)α$^+$), (9) LSK cells (CD45$^+$Lin2$^-$KIT$^+$Sca1$^+$), (10) LK cells (CD45$^+$Lin2$^-$KIT$^+$Sca1$^-$), (11) granulocyte-macrophage progenitor (CD 45$^+$Lin2$^-$KIT$^+$Sca1$^-$CD34$^+$CD16/32^{high}CD115$^-$), (12) monocyte-dendritic cell progenitor (CD45$^+$Lin2$^-$KIT$^+$Sca1$^-$CD34$^+$CD16/32^{high}CD115$^+$), (13) pre-pro B cells (Lin3$^-$B220^{int}CD93$^+$IgM$^-$CD19$^-$), (14) pro B cells (Lin3$^-$B220^{int}CD93$^+$IgM$^-$CD19$^+$CD43$^+$CD24$^+$), (15) pre B cells (Lin3$^-$B220^{int}CD93$^+$IgM$^-$CD19$^+$CD43$^-$CD24$^+$), (16) IgM B cells (Lin3$^-$B220^{int}CD93$^+$IgM$^+$CD19$^+$), (17) mature B cells (Lin3$^-$B220^{int}IgD$^+$). Lineages were defined as: Lin1: CD3, NK1.1, CD90.2, CD19; Lin2: CD90.2, CD3, CD19, Ly-6G, Ly-6C, NK1.1, CD11c; (Lin2 for BrdU staining: B220, CD19, CD49b, Ter119, CD90.2, CD11b, CD11c, Ly-6G, IL7Ra); Lin3: CD4, CD8, CD3, NK1.1, CD11b, Ly-6G. Data were acquired using a LSRII (BD Biosciences) and analysed with FlowJo (Tree Star).

BrdU proliferation assays.—To analyse cell proliferation, 2 mg BrdU was intraperitoneally injected 4 h before the mice were euthanized. BrdU$^+$ cells were stained using a BrdU flow kit (BD Biosciences) according to the manufacturer's instructions.

RNA and protein assays

PCR.—Total RNA was isolated using the RNeasy Mini Kit (Qiagen) or the MicroElute Total RNA Kit (Omega Bio-tek) according to the manufacturer's instructions. RNA quality and quantity were determined using the NanoDrop (Thermo Fisher Scientific) system. The High Capacity cDNA Reverse Transcription Kit (Applied Biosystems) was used to generate cDNA from up to 1 μg of total RNA per sample. The following TaqMan primers (Applied Biosystems) were used for quantitative realtime TaqMan PCR: *Gapdh* (Mm99999915_g1), *Actb* (Mm00607939_s1), *Cxcr4* (Mm01996749_s1), *Cxcl1* (Mm04207460_m1), *Nr3c1* (Mm00433832_m1). TaqMan PCR was performed on a 7500 thermal cycler (Applied Biosystems). Gene expression was normalized to *Actb* or *Gapdh* and quantified using the $2^{-\Delta\Delta C_t}$ method.

Bulk RNA-seq.—For bulk RNA-seq, blood neutrophils (each sample pooled from $n = 3$ mice) were FACS sorted (CD45$^+$Lin$^-$CD11b$^+$Ly-6G$^+$) into empty 1.5 ml tubes ($n = 4$ samples per group, total of $n = 36$ mice). After centrifugation, the supernatant was removed and the cell pellet was lysed in RLT lysis buffer, from the RNeasy Micro Kit (Qiagen), containing 1% β-mercaptoethanol. The RNeasy Micro Kit (Qiagen) was subsequently used to extract the RNA according to the manufacturer's instructions. RNA-seq libraries were constructed from total RNA using the Clontech SMARTer v4 kit (Takara), followed by sequencing on an Illumina HiSeq 2500 instrument, resulting in 20–30 million 50 bp reads per sample. The STAR aligner[42] was used to map sequencing reads to transcriptome in the mouse mm9 reference genome. Read counts for individual genes were produced using the unstranded count function in HTSeq (v.0.6.0)[43], followed by estimating expression values and detecting differentially expressed transcripts using EdgeR[44], which included only the genes with counts per million reads (CPM) > 1 for one or more samples[45]. Differentially expressed genes were defined by at least a twofold change in the average expression value with a false-discovery rate (FDR) < 0.05. RNA-seq data have been deposited for public access at the NCBI Gene Expression Omnibus (GEO) database under accession number GSE201392.

scRNA-seq.—For scRNA-seq, neutrophils were FACS sorted (CD45$^+$Lin$^-$CD11b$^+$Ly-6G$^+$) into 1.5 ml tubes. After cell counting and viability control, a scRNA-seq library was constructed on the Chromium 10x instrument using Chromium single cell 3′ reagent v3.0 kits, followed by sequencing on the Illumina HiSeq 2500 instruments, which resulted in approximately 205–209 million reads per sample.

scRNA-seq data analysis.—scRNA-seq sequencing data were initially processed using CellRanger (v.4.0.0) (https://support.10xgenomics.com/single-cell-gene-expression/software/overview/welcome). In brief, reads were aligned to the mm10 mouse reference genome with a mapping rate of around 60%, followed by the generation of read counts per gene in each cell. Further analysis was performed using the Seurat v.3.2.3 package[46]. We filtered out cells with <200 expressed genes and genes expressed in <3 cells, then excluded cells with high mitochondrial transcript content (>10% of total reads). Counts across all cells for each sample were normalized using the NormalizeData() function. Using the FindVariableFeatures() function, we selected 2,000 features to be used in a principal component analysis. UMAP dimensionality reduction and cell clustering were performed using the RunUMAP() and FindClusters() functions, respectively. The VlnPlot() and FeaturePlot() functions were used to generate violin plots and feature plots for the datasets. Heat maps of gene expression were generated using the DoHeatmap() function. Cells from all samples were then integrated using the Seurat canonical correlation analysis (CCA) method. Integration anchors were obtained using the FindIntegrationAnchors() function and used to integrate individual datasets with the IntegrateData() function. Biological annotation of cell clusters was based on the expression of known cell type markers. For the analysis of differential expression, the FindMarkers() function was applied to the integrated samples to identify differentially expressed genes between the cell subsets of interest. After the initial Seurat integration analysis, the SubsetData() function was used to subset a more pure population of neutrophils for further analysis. The similarity between clusters defined in this

work (0 to 3) and clusters defined in ref.[34] (G0 to G5c) was calculated using the fastMNN Seurat wrapper[47]. Similarity scores were visualized as a heat map using morpheus (https://software.broadinstitute.org/morpheus). Maturation scores were derived on the basis of the set of neutrophil maturation genes defined in ref.[34]. For each individual gene, expression values were scaled by calculating Z-scores based on the distribution of expression values across all cells. The average Z-score for all genes in the set was calculated for each cell. These average Z-scores were visualized as a violin plot among individual conditions. RNA-seq data have been deposited for public access at the NCBI GEO database under accession number GSE201392.

Multi cytokine/chemokine array.—A membrane-based antibody array (Proteome Profiler Mouse Cytokine Array Kit, Panel A, R&D Systems) was used according to the manufacturer's instructions to simultaneously determine the relative levels of 40 mouse cytokines and chemokines in blood plasma of non-stressed versus 1 h restraint-stressed mice.

Corticosterone ELISA.—Blood plasma corticosterone levels were measured using a commercial corticosterone ELISA kit (Abcam, ab108821) according to the manufacturer's instructions.

CXCL1 ELISA.—Blood serum CXCL1 levels were measured using a commercial CXCL1 ELISA kit (Mouse CXCL1/KC Quantikine ELISA Kit, R&D Systems) according to the manufacturer's instructions. For quantification of muscle CXCL1, skeletal muscle was homogenized in RIPA buffer in bead-homogenizer tubes. After centrifugation, CXCL1 levels in the supernatant were quantified using the same ELISA kit.

IL-16 ELISA.—Blood serum IL-16 levels were measured using a commercial IL-16 ELISA kit (Mouse IL-16 ELISA Kit, Novus Biologicals) according to the manufacturer's instructions.

Myoglobin ELISA.—Blood serum myoglobin levels were measured using a commercial myoglobin ELISA kit (Mouse Myoglobin ELISA Kit, Abcam) according to the manufacturer's instructions.

Inffluenza-specific antibodies.—For ELISA, BAL anti-IAV IgG1 was measured by a modified ELISA. In brief, 96-well ELISA plates (Corning) were coated with 1.25×10^7 PFU per ml ultraviolet-light-inactivated IAV A/ PR/8/34 in PBS and incubated at room temperature overnight. The wells were then blocked with blocking buffer (1% BSA in PBS) for 2 h at room temperature. The plates were washed, and undiluted BAL samples were added and incubated at room temperature for 2 h. After the washes, HRP-conjugated goat anti-mouse IgG1 was added to the wells for 2 h at room temperature. The plates were again washed and TMB substrate was added for 20 min in the dark. Reactions were then stopped with 2 N H_2SO_4 and optical density values were obtained at 450 nm.

Histology.—After transcardiac perfusion with PBS and formalin (10% formalin solution, Fisher Chemical), brains were carefully removed from the skulls and post-fixed in formalin

overnight. Fixed brains were transferred into 0.8 M sucrose for cryoprotection and cut into predefined coronal blocks. These blocks were embedded in Tissue-Tek OCT compound, frozen in dry-ice-cooled 2-methylbutane and cryo-sectioned into 50-μm-thick sections. Series (200 μm apart) of free-floating coronal brain sections were washed in PBS and pretreated with 1% sodium borohydride (Sigma-Aldrich) in PBS for 15 min. After repeated washes in PBS, the sections were preincubated in a solution containing 10% normal horse serum (Sigma-Aldrich), 0.3% Triton X-100 (Sigma-Aldrich) and 0.05% phenylhydrazine (Sigma-Aldrich) in PBS for 30 min. Subsequently, the sections were incubated in a solution containing 10% normal horse serum, 0.3% Triton X-100, 0.1% sodium azide (Sigma-Aldrich), and the appropriately diluted primary antibody or antibody mixture overnight at 4 °C (rat anti-mCherry, M11217, Invitrogen, 1:1,000; rabbit anti-GFP, A-11122, Invitrogen, 1:1,000; rabbit anti-FOS, F7799, Sigma-Aldrich, 1:20,000). After two wash steps in PBS (20 min and 40 min) and preincubation in BSA(Sigma-Aldrich) supplemented PBS (2 mg BSA per ml PBS; PBS-A) for 60 min, the sections were incubated in a solution containing 0.3% Triton X-100, 0.1% sodium azide, and the appropriately diluted secondary antibody or antibody mixtures (AF594 goat anti-rat, A-11007, Invitrogen, 1:500; AF488 goat anti-rabbit, A-11008, Invitrogen, 1:500; biotinylated goat anti-rabbit, BA-1000, Vector Labs, 1:1,000) in PBS-A for 2–4 h at room temperature in the dark. After washing in PBS, fluorescence-stained sections were mounted on gelatin-coated slides (Cole-Parmer), air dried to firmly attach to the slide, rehydrated in PBS and then cover-slipped using mounting medium (Vectashield HardSet Antifade Mounting Medium, Vector Laboratories). Sections that were stained with the secondary biotinylated goat anti-rabbit antibody were washed in PBS, preincubated in PBS-A and incubated for 2–4 h in ABC solution (Vectastain Elite ABC HRP Kit, PK-6100, Vector Labs, 1:200 in PBS-A). After washing in PBS, the sections were incubated in a 3,3′-diaminobenzidine (DAB) solution (1.4 mM DAB, 10 mM imidazole in 0.05 M Tris buffer, pH 7.6) for 15 min before colour development was started by adding 0.03% hydrogen peroxide to the DAB solution. After 15–20 min, the colour reaction was stopped by repeated washing in PBS. The stained sections were mounted onto gelatin-coated slides (Cole-Parmer), air dried to firmly attach to the slides, dehydrated through a graded ethanol series, transferred into a xylenes solution (Sigma-Aldrich) and then cover-slipped with Entellan (Sigma-Aldrich). Aortic roots were collected, embedded and sectioned for immunofluorescence staining. Ly-6G antibodies (1A8, 127602, BioLegend) were incubated at 4 °C overnight, and a biotinylated secondary antibody followed by streptavidin-DyLight 594 (BA4001 and SA-5594, Vector Laboratories) were used to detect neutrophils. Nuclei were counterstained with DAPI (D21490, Thermo Fisher Scientific) and sections were scanned using a digital slide scanner (NanoZoomer 2.0-RS). For lung histology, lungs were perfused, inflated and fixed for 48 h with 10% formalin, then embedded in paraffin. Next, 5 μm sections were cut and stained with haematoxylin and eosin. Slides were scanned at ×40 magnification and pictures were taken using a Leica Aperio slide scanner.

Statistics

Results are presented as mean ± s.e.m. Statistical tests were performed using GraphPad Prism 8 and included unpaired two-tailed Student's *t*-tests (two groups) and nonparametric Mann-Whitney *U*-tests (when Gaussian distribution was not assumed). For multiple comparisons, non-parametric multiple-comparison tests comparing the mean rank of each

group (when Gaussian distribution was not assumed), or one- or two-way ANOVA followed by Dunnett multiple-comparisons test for one-way ANOVA and Sidak multiple-comparisons test for two-way ANOVA were used. Survival curves were analysed using the log-rank (Mantel–Cox) test. $P < 0.05$ was considered to be statistically significant; $*P < 0.05$, $**P < 0.01$, $***P < 0.001$.
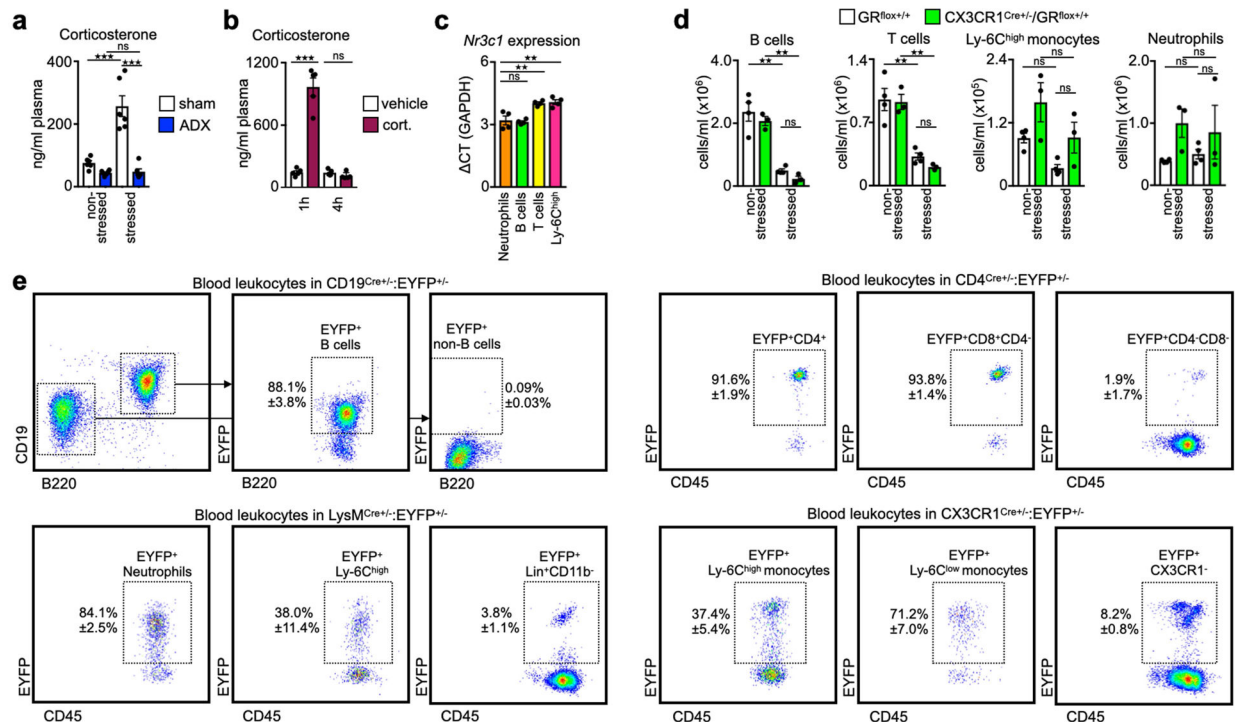
Extended Data
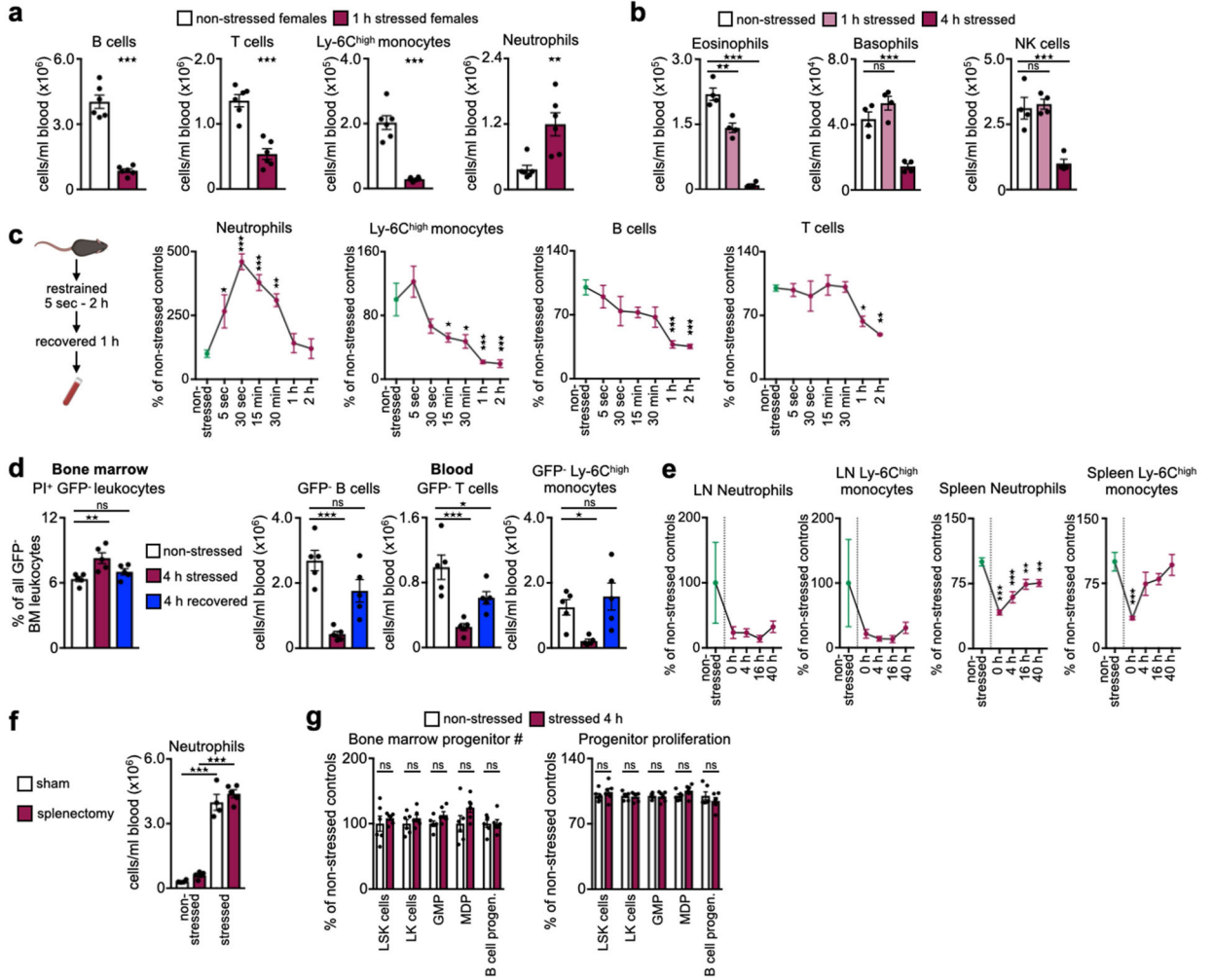
Extended Data Fig. 1 |. Acute psychological stress induces large-scale bidirectional leukocyte shifts.

a, Quantification of circulating blood leukocytes after 1 h of restraint stress in female WT mice (n = 6 per group). Two-tailed unpaired t-test. **b**, Quantification of circulating blood eosinophils, basophils, and NK cells after 1h and 4h of restraint stress (n = 4 per group). One-way ANOVA. **c**, Quantification of circulating blood neutrophils, Ly-6C^high monocytes, B cells, and T cells 1 h after cessation of a restraint stress episode with the indicated duration (expressed as percentage of the mean of non-stressed control mice, n = 4 mice per time point). One-way ANOVA. **d**, Analyses of endogenous GFP⁻ leukocytes from the GFP⁺ leukocyte transfer experiment shown in Fig. 1e. Assessment of cell death of endogenous

GFP⁻ leukocytes in the bone marrow of recipient mice under non-stressed conditions, after restraint stress, and during stress recovery (PI⁺ GFP⁻ leukocytes in % of all bone marrow leukocytes; PI - propidium iodide). Quantification of endogenous GFP⁻ leukocytes in the blood of recipient mice under non-stressed conditions, after restraint stress, and during stress recovery (n = 5 mice per group). One-way ANOVA. **e**, Neutrophil and Ly-6C^{high} monocyte numbers in inguinal lymph nodes (LN) and spleen measured after the indicated time of recovery from one 4 h restraint stress episode (expressed as percentage of the mean of non-stressed control mice, n = 4 mice in non-stressed LN analyses, otherwise n = 5 mice). One-way ANOVA. B cell and T cell data from the same experiment are shown in Fig. 1f. **f**, Quantification of circulating blood neutrophils under non-stressed baseline conditions and 40 min after cessation of a 20-min restraint stress episode in splenectomized versus sham-operated mice (n = 4 sham-operated mice, n = 5 splenectomized mice). Two-way ANOVA. **g**, Quantification of bone marrow progenitor cell numbers under non-stressed conditions and after one 4 h restraint stress episode expressed as percentage of the mean cell number of non-stressed control mice (n = 6 per group). Determination of bone marrow progenitor cell proliferation (4h BrdU pulse) under non-stressed conditions and after one 4 h restraint stress episode expressed as percentage of the mean proliferation rate of non-stressed control mice (n = 6 per group). Two-tailed unpaired t-test. Data are mean ±s.e.m.; ★P < 0.05, ★★P < 0.01, ★★★P < 0.001, statistical tests used as indicated.

Extended Data Fig. 2 |. The paraventricular hypothalamus controls leukocyte homing to the bone marrow during stress.

a, Quantification of plasma corticosterone levels in adrenalectomized (ADX) and sham-operated mice at baseline and after 4 h of restraint stress (n = 6 mice per group). Two-way ANOVA. **b**, Quantification of plasma corticosterone levels 1 h and 4 h after

intraperitoneal injection of vehicle or corticosterone (5mg/kg) into WT mice (n = 5 mice per group). Two-way ANOVA. **c**, Transcript expression of *Nr3c1* (GR) on sorted blood leukocytes expressed as CT compared to the house-keeping gene *Gapdh* (CT_{mean} *Nr3c1* - CT_{mean} *Gapdh*) (sorted cells from n = 4 samples, each sample pooled from n = 4 WT mice). One-way ANOVA. **d**, Quantification of circulating blood leukocytes in mice with CX3CR1^Cre-driven knockout of the glucocorticoid receptor (CX3CR1^{Cre+/−}:GR^{flox+/+}) and control mice (GR^{flox+/+}) at baseline and after 4 h of restraint stress (n = 3 CX3CR1^{Cre+/−}:GR^{flox+/+} mice, and n = 4 GR^{flox+/+} mice). Two-way ANOVA. **e**, Gating strategies and percentages of cells expressing enhanced yellow fluorescent protein (EYFP+) within the indicated blood leukocyte populations in CD19^{Cre+/−}:EYFP^{+/−} reporter mice (n = 4), LysM^{Cre+/−}:EYFP^{+/−} reporter mice (n = 12), CD4^{Cre+/−}:EYFP^{+/−} reporter mice (n = 3), and CX3CR1^{Cre+/−}:EYFP^{+/−} reporter mice (n = 2). Data are mean ±s.e.m.; ★P < 0.05, ★★P < 0.01, ★★★P < 0.001, statistical tests used as indicated.
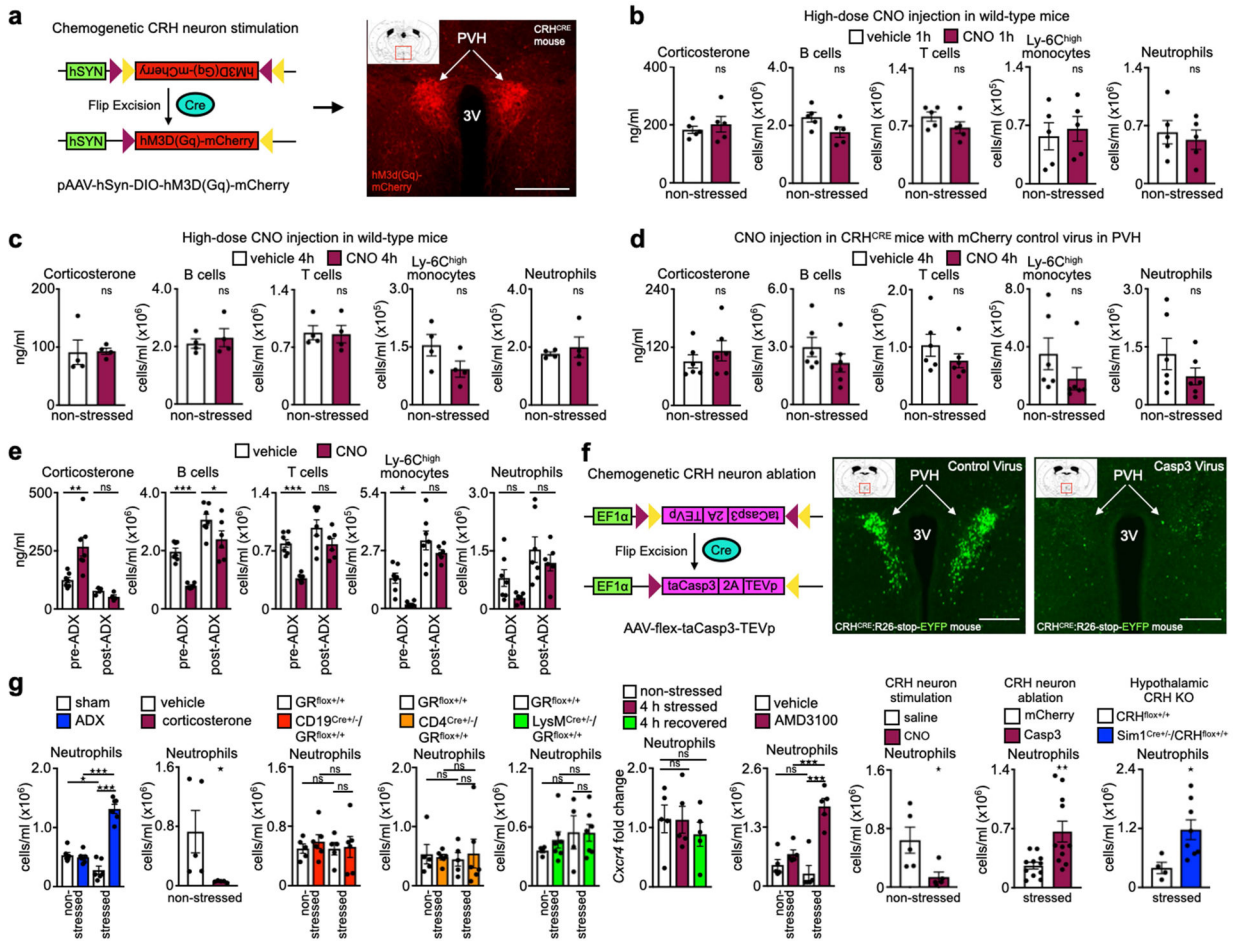
Extended Data Fig. 3 |. Leukocyte homing during stress.
a, Schematic of Cre-mediated flip-excision activation of the activating chemogenetic virus pAAV-hSyn-DIO-hM3D(Gq)-mCherry. Representative injection site of pAAV-hSyn-DIO-hM3D(Gq)-mCherry in the PVH of a CRH^Cre mouse stained with anti-mCherry primary antibody and AF594-labelled secondary antibody (PVH, paraventricular hypothalamus; 3V,

third ventricle). Scale bar indicates 400 μm. **b,** Determination of plasma corticosterone levels and quantification of circulating blood leukocytes 1 h after high-dose intraperitoneal injection of clozapine-N-oxide (CNO) versus vehicle in WT mice (n = 5 mice per group). Two-tailed unpaired t-test. **c,** Determination of plasma corticosterone levels and quantification of circulating blood leukocytes 4 h after high-dose intraperitoneal injection of clozapine-N-oxide (CNO) versus vehicle in WT mice (n = 4 mice per group). Two-tailed unpaired t-test. **d,** Determination of plasma corticosterone levels and quantification of circulating blood leukocytes 4 h after intraperitoneal injection of clozapine-N-oxide (CNO) versus vehicle in CRH[Cre] mice that had previously received an mCherry control virus injection into the PVH (two experiments with changed groups combined, total of n = 6 mice per group). Two-tailed unpaired t-test. **e,** Determination of plasma corticosterone levels and quantification of circulating blood leukocytes 5 h after injection of vehicle or CNO into CRH[Cre] mice that had received an hM3D(Gq) injection into the PVH 3 weeks prior, pre- and post adrenalectomy (ADX) (leukocyte analyses: n = 7 pre-ADX vehicle, n = 6 pre-ADX CNO, n = 7 post-ADX vehicle, n = 6 post-ADX CNO; corticosterone analyses: n = 7 pre-ADX vehicle, n = 7 pre-ADX CNO, n = 3 post-ADX vehicle, n = 4 post-ADX CNO)Two-way ANOVA. **f,** Schematic of Cre-mediated flip-excision activation of the apoptosis-inducing virus AAV-flex-taCasp3-TEVp. Representative images of the PVH of CRH[Cre]:R26-stop-EYFP mice injected with either pAAV-hSyn-DIO-hM3D(Gq)-mCherry control virus (left image) or AAV-flex-taCasp3-TEVp ablating virus (right image) stained with anti-GFP primary antibody and AF488-labelled secondary antibody (PVH, paraventricular hypothalamus; 3V, third ventricle). Scale bars indicate 250 μm. **g,** Quantification of circulating blood neutrophils in the experiments presented in Fig. 2a–2g and 2i–2k (n numbers indicated in Fig. 2a–2g and 2i–2k). Two-way ANOVA or unpaired t-test as appropriate. Data are mean ±s.e.m.; ★P < 0.05, ★★P < 0.01, ★★★P < 0.001, statistical tests used as indicated.
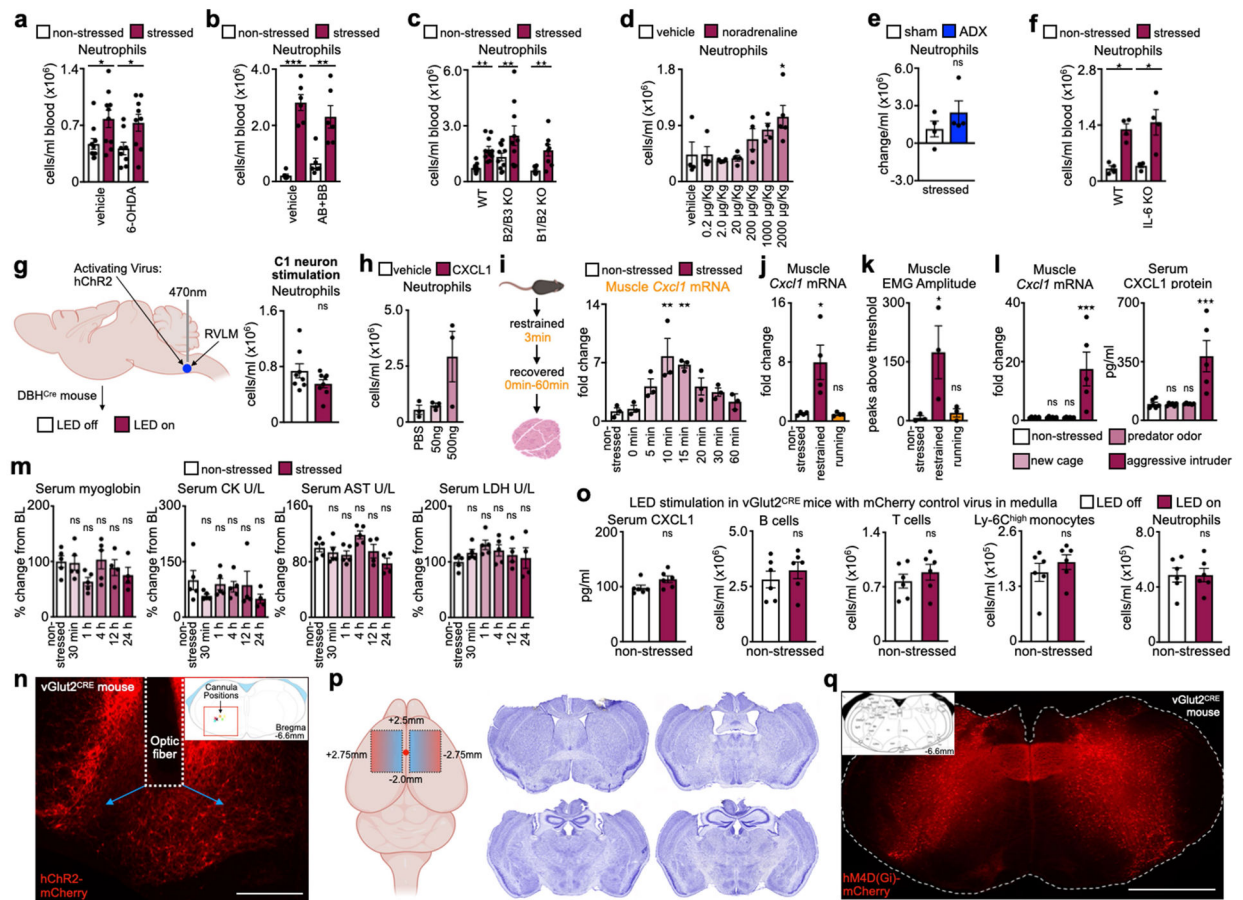
Extended Data Fig. 4 |. Central motor circuits control neutrophil egress from the bone marrow during acute stress.

a, Quantification of circulating blood neutrophils under non-stressed conditions and after 1 h of restraint stress in sympathectomized (6-OHDA) vs. vehicle-treated mice (2 experiments combined, n = 10 non-stressed vehicle-treated mice, n = 10 non-stressed 6-OHDA-treated mice, n = 8 stressed vehicle-treated mice, n = 8 stressed 6-OHDA-treated mice). Two-way ANOVA. **b**, Quantification of circulating blood neutrophils under non-stressed conditions and 40 min after a 20 min restraint stress episode in high-dose alpha-(phentolamine, 30mg/Kg) and beta-adrenergic receptor blocker (propranolol, 30mg/Kg) vs. vehicle-treated mice (n = 6 per group). The non-stressed baseline was collected 75 min after the i.p. injection of vehicle or alpha-$^{/-}$and beta-blocker. Two-way ANOVA. **c**, Quantification of circulating blood neutrophils under non-stressed conditions and after 1 h of restraint stress in WT mice, beta 2/beta 3 adrenergic receptor double knockout mice (B2/B3 KO), and beta 1/beta 2 adrenergic receptor double knockout mice (B1/B2 KO) (n = 11 WT mice, n = 10 B2/B3 KO mice, n = 8 B1/B2 KO mice). The non-stressed baseline was collected from the same mice one week apart from the actual stress experiment, at the same time of the day. Data from the B1/B2 KO mice were generated in an independent experiment. Two-way ANOVA. **d**, Quantification of circulating blood neutrophils in WT mice 1 h after injection of vehicle or the indicated doses of noradrenaline (n = 5 in the 2000μg/Kg group, n = 4 in all other groups). One-way ANOVA. **e**, Change in circulating blood neutrophil numbers

induced by 1 h of restraint stress in adrenalectomized (ADX) vs. sham-operated WT mice (calculated as neutrophil number after 1h h of stress - leukocyte number at baseline; n = 4 mice per group). Unpaired t-test. **f**, Quantification of circulating blood neutrophils under non-stressed conditions and after 1 h of restraint stress in WT mice vs. interleukin-6 (IL-6) knockout mice (n = 4 per group). Two-way ANOVA. **g**, Schematic of optogenetic approach used to stimulate hChR2-expressing neurons in the rostroventrolateral medulla (RVLM) of DBH Cre mice. Quantification of circulating blood neutrophils 55 min after a 5 min LED stimulation period compared to hChR2-injected DBH^{Cre} mice without light stimulation (cross-over design with each mouse analysed with and without LED stimulation 1d apart, total of n = 8 per group). Two-tailed unpaired t-test. **h**, Quantification of circulating blood neutrophils in WT mice 1 h after injection of vehicle or the indicated doses of CXCL1 (n = 3 per group). **i**, *Cxcl1* transcript expression in the gluteal muscle measured after the indicated time of recovery from a 3 min restraint stress episode (expressed as fold change from non-stressed control mice, n = 3 mice per time point). One-way ANOVA. **j**, *Cxcl1* transcript expression in the gluteal muscle measured immediately after 1 h of restraint stress vs voluntary running on a running wheel compared to non-stressed control mice without a running wheel (n = 4 per group). One-way ANOVA. **k**, Wireless EMG telemetry recordings from the gluteal and upper leg musculature in WT mice under conditions of restraint stress vs voluntary running on a running wheel compared to non-stressed controls without a running wheel (each mouse was recorded under each condition on subsequent days during their active period, data expressed as number of amplitude peaks above a mouse-specific threshold of 0.2 mV (2 mice) or 0.4 mV (1 mouse) during the first 10min of restraint) (n = 3 mice total, each recorded under each condition as outlined above). One-way ANOVA. **l**, *Cxcl1* transcript expression in the gluteal muscle and CXCL1 protein levels in the serum measured in WT mice immediately after 1 h of exposure to the indicated stressor compared to non-stressed controls (*Cxcl1* transcript expression expressed as fold change from non-stressed control mice (n = 5 in the aggressive intruder group, n = 6 in all other groups). One-way ANOVA. **m**, Muscle damage parameters in blood serum at different time points after the onset of a 30 min restraint stress episode, compared to non-stressed controls. Serum myoglobin measured by ELISA. Serum creatine kinase (CK), aspartate aminotransferase (AST), and lactate dehydrogenase (LDH) activities in units/liter (U/L) were determined by IDEXX BioAnalytics (n = 5 non-stressed mice, n = 5 mice 30min post stress onset, n = 5 mice 1h post stress onset, n = 5 mice 4h post stress onset, n = 4 mice 12h post stress onset, n = 4 mice 24h post stress onset). One-way ANOVA. **n**, Representative injection site of the channelrhodopsin encoding virus pAAV-EF1a-double floxed-hChR2(H134R)-mCherry-WPRE-HGHpA with optic fibre position in the medulla of a vGlut2^{Cre} mouse stained with anti-mCherry primary antibody and AF594-labelled secondary antibody. Optic cannula positions indicated in the inset. Scale bar indicates 500 μm. **o**, CXCL1 protein levels in the serum and circulating blood leukocyte numbers measured immediately after 30 min of LED stimulation (LED on) compared no-LED stimulation (LED off) in vGlut2^{Cre} mice that had previously received an mCherry control virus injection with cannula implantation into the medulla (two experiments with changed groups combined, total of n = 6 mice per group). Two-tailed unpaired t-test. **p**, Schematic of the bilateral motor cortex ablation approach with coordinates indicated as distance from Bregma. Representative Cresyl Violet stained brain sections showing the extend of ablation. **q**, Representative bilateral injection sites of the

inhibitory DREADD encoding virus pAAV-hSyn-DIO-hM4D(Gi)-mCherry in the medulla of a vGlut2^{Cre} mouse stained with anti-mCherry primary antibody and AF594-labelled secondary antibody. Scale bar indicates 1000 μm. Data are mean ±s.e.m.; ★P < 0.05, ★★P < 0.01, ★★★P < 0.001, statistical tests used as indicated.
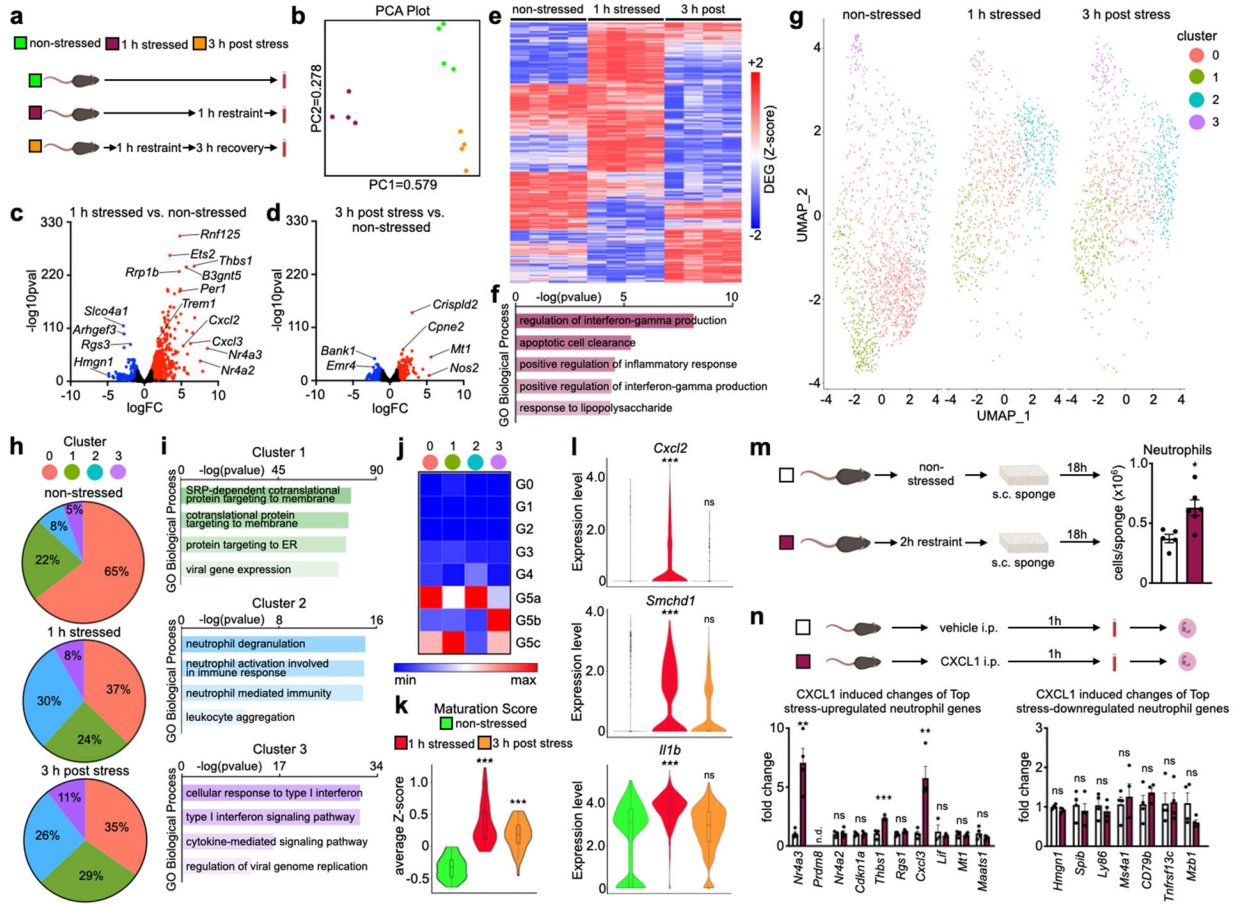
Extended Data Fig. 5 |. Acute stress induces neutrophil reprogramming and their recruitment to wounds.

a, Schematic of experimental approach. **b**, Principal component analysis (PCA) plot of RNAseq data of blood neutrophils (CD45$^+$; Lin$^-$; CD11b$^+$; Ly-6G$^+$) sorted from WT mice under non-stressed conditions, after 1 h of restraint stress, and 3 h after a 1 h restraint stress episode (n = 4 samples per group, each sample pooled from 3 mice, total 36 mice). **c**, Volcano plot indicating differentially regulated genes (FC > 2.0, FDR < 0.05, p < 0.05) in blood neutrophils from 1 h stressed versus non-stressed mice. **d**, Volcano plot indicating differentially regulated genes (FC > 2.0, FDR < 0.05, p < 0.05) in blood neutrophils from mice 3 h post stress versus non-stressed mice. **e**, Heatmap of differentially expressed genes in blood neutrophils sorted from WT mice under non-stressed conditions, after 1 h of restraint stress, and 3 h after a 1 h restraint stress episode (n = 4 mice per group). **f**, Pathway analysis of significantly regulated genes between 1 h stressed versus non-stressed (FC > 2.0, FDR < 0.05, p < 0.05) using the Enricher with GO Biological Process 2018. **g**, Uniform manifold approximation and projection (UMAP) plots of single-cell RNAseq

data of blood neutrophils (CD45$^+$; Lin$^-$; CD11b$^+$; Ly-6G$^+$) sorted from non-stressed as well as 1 h-stressed and 1h-stressed plus 3 h-recovered mice revealing 4 different neutrophil clusters. **h,** The four neutrophil clusters' relative contributions to the overall blood neutrophil population under non-stressed conditions and in response to stress and recovery. **i,** Pathway analysis of the different clusters based on the top 50 cluster-defining genes using the Enricher with GO Biological Process 2018. **j,** Heatmap comparing the similarities between the four peripheral blood neutrophil clusters defined in our study with those described in a recent single-cell analysis of neutrophil heterogeneity in blood (G5a-G5c) and bone marrow (G0-G4)[34]. **k,** Neutrophil maturation score determined based on the expression of maturation-related genes[34]. One-way ANOVA. Violin plots show **l,** Violin plots showing the expression levels of key neutrophil products including *Cxcl2, Smchd1,* and *Il1b* under non-stressed conditions and in response to stress and recovery. One-way ANOVA. Violin plots show **m,** Schematic of experimental approach used to test the effect of acute stress on neutrophil recruitment into a sterile subcutaneous sponge. Quantification of neutrophils in the sponge (18h after implantation) in WT mice that were either stressed for 2h immediately prior to the sponge implantation or remained non-stressed (n = 5 non-stressed, n = 6 restraint stressed). **n,** Schematic of experimental approach used to sort blood neutrophils 1 h after intraperitoneal injection of CXCL1 (500 ng) or vehicle. Transcript expression analyses of the top up- and down-regulated genes in response to stress identified in the bulk RNA sequencing experiment (non-stressed vs. 1h stressed) 1 h after injection of CXCL1 versus vehicle in non-stressed mice (transcript expression expressed as fold change from vehicle-injected control mice; n = 4 samples per group, each pooled from 3 WT mice, total 24 mice). Unpaired t-test. Data are mean ±s.e.m.; ★$P < 0.05$, ★★$P < 0.01$, ★★★$P < 0.001$, statistical tests used as indicated.
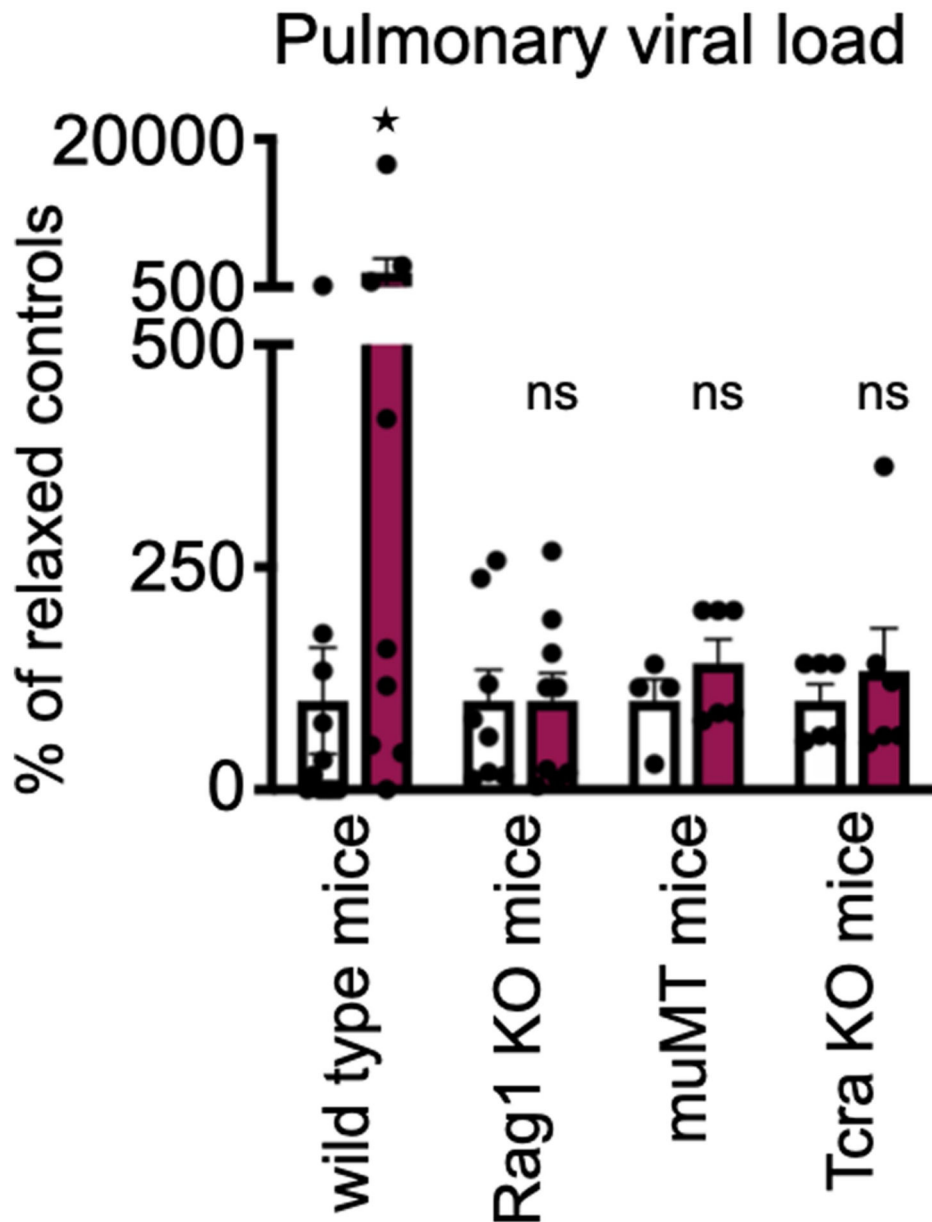
Extended Data Fig. 6 |. Requirement of B and T cells in stress-induced changes in viral titres after IAV infection.

Standard MDCK plaque assay determined viral load in the lungs of stressed versus non-stressed (stress scheme outlined in Fig. 5e) WT mice, Rag1 KO mice, muMT mice, and Tcra KO mice on day 9 post IAV infection, expressed as percentage of the average of the respective non-stressed control mice (n = 11 non-stressed WT mice and n = 9 stressed WT mice, two experiments compiled; n = 8 non-stressed Rag1 KO mice and n = 9 stressed Rag1 KO mice, two experiments compiled; n = 4 non-stressed muMT mice and n = 6 stressed muMT mice, n = 6 non-stressed Tcra KO mice and n = 6 stressed Tcra KO mice). Two-tailed Mann-Whitney test.
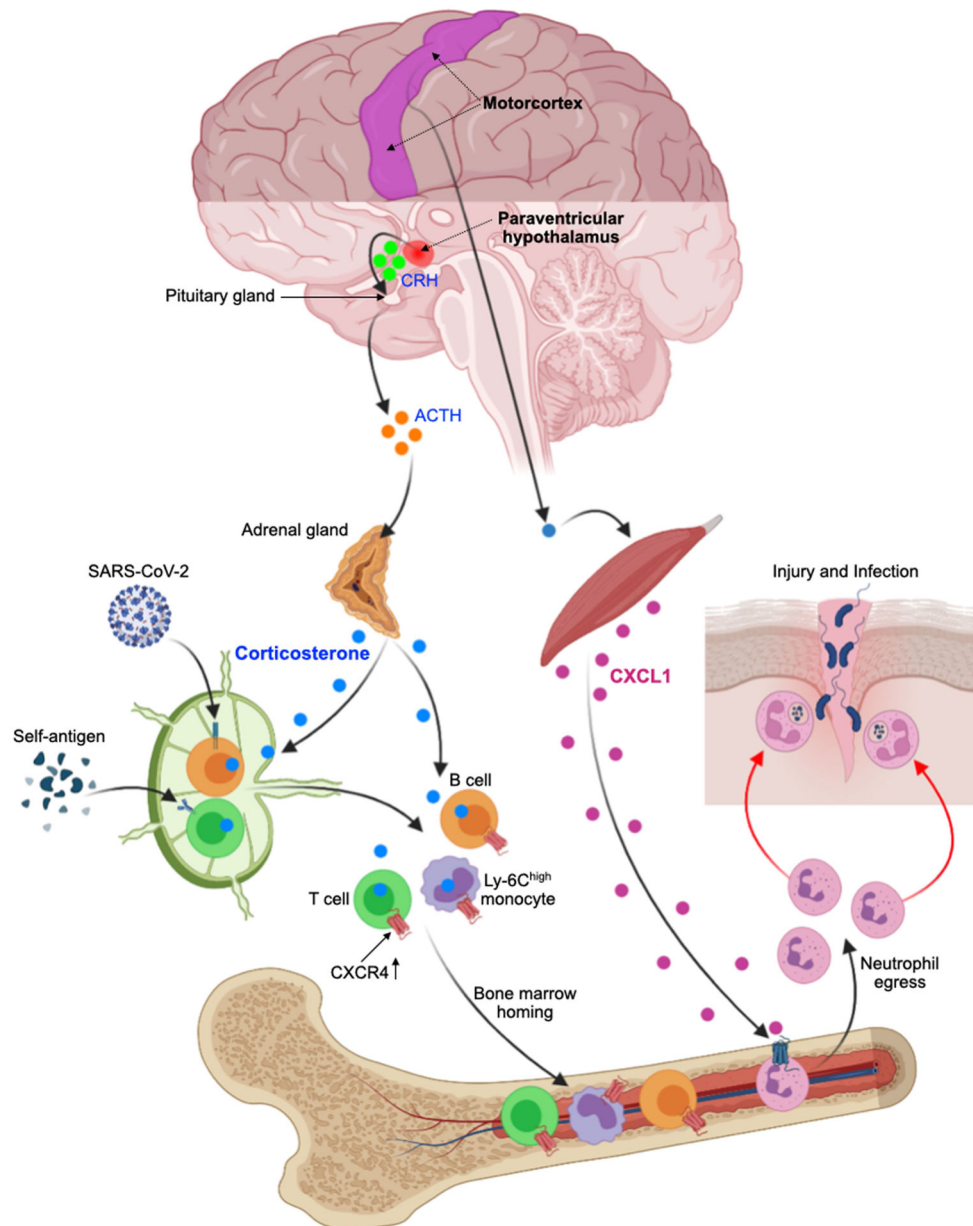
Extended Data Fig. 7 |. Brain motor and fear circuits differentially regulate leukocyte distribution and function during acute stress.

Model of brain-immune interactions and their consequences during acute stress. The motor cortex induces rapid neutrophil mobilization from the bone marrow to peripheral tissues and atherosclerotic plaques via skeletal muscle derived neutrophil-attracting chemokine CXCL1. Conversely, the paraventricular hypothalamus controls lymphocyte and monocyte migration from blood and secondary lymphoid organs to the bone marrow through leukocyte-intrinsic glucocorticoid signalling, thereby altering the acquisition of adaptive immunity to viral infections and self antigens. Figure created with BioRender. com. Abbreviations: CRH - corticotropin releasing hormone; ACTH - adrenocorticotropic hormone; CXCR4 - C-X-C chemokine receptor type 4; CXCL1 - chemokine (C-X-C motif) ligand 1.

Acknowledgements

Data availability

All data supporting the findings of this study are available within the Article or will be publicly available on publication. Bulk and single-cell RNA-seq data of blood neutrophils have been deposited for public access at the NCBI GEO database under accession number GSE201392. Source data are provided with this paper.

References

1. Schiller M, Ben-Shaanan TL & Rolls A Neuronal regulation of immunity: why, how and where. Nat. Rev. Immunol 21, 20–36 (2021). [PubMed: 32811994]

2. Dhabhar FS, Malarkey WB, Neri E & McEwen BS Stress-induced redistribution of immune cells– from barracks to boulevards to battle ields: a tale of three hormones–Curt Richter Award winner. Psychoneuroendocrinology 37, 1345–1368 (2012). [PubMed: 22727761]

3. Poller WC, Nahrendorf M & Swirski FK Hematopoiesis and cardiovascular disease. Circ. Res 126, 1061–1085 (2020). [PubMed: 32271679]

4. Chervenick PA, Boggs DR, Marsh JC, Cartwright GE & Wintrobe MM Quantitative studies of blood and bone marrow neutrophils in normal mice. Am. J. Physiol 215, 353–360 (1968). [PubMed: 5665168]

5. Colvin GA et al. Murine marrow cellularity and the concept of stem cell competition: geographic and quantitative determinants in stem cell biology. Leukemia 18, 575–583 (2004). [PubMed: 14749701]

6. Glaser R & Kiecolt-Glaser JK Stress-induced immune dysfunction: implications for health. Nat. Rev. Immunol 5, 243–251 (2005). [PubMed: 15738954]

7. Shimba A et al. Glucocorticoids drive diurnal oscillations in Tflcell distribution and responses by inducing interleukin-7 receptor and CXCR4. Immunity 48, 286–298 (2018). [PubMed: 29396162]

8. Besedovsky L, Born J & Lange T Endogenous glucocorticoid receptor signaling drives rhythmic changes in human T-cell subset numbers and the expression of the chemokine receptor CXCR4. FASEB J. 28, 67–75 (2014). [PubMed: 24051033]

9. Cain DW et al. Murine glucocorticoid receptors orchestrate B cell migration selectively between bone marrow and blood. J. Immunol 205, 619–629 (2020). [PubMed: 32571841]

10. Collins N et al. The bone marrow protects and optimizes immunological memory during dietary restriction. Cell 178, 1088–1101 (2019). [PubMed: 31442402]

11. Okutsu M, Ishii K, Niu KJ & Nagatomi R Cortisol-induced CXCR4 augmentation mobilizes T lymphocytes after acute physical stress. Am. J. Physiol. Regul. Integr. Comp. Physiol 288, R591–R599 (2005). [PubMed: 15528395]

12. Senba E, Matsunaga K, Tohyama M & Noguchi K Stress-induced c-fos expression in the rat brain: activation mechanism of sympathetic pathway. Brain Res. Bull 31, 329–344 (1993). [PubMed: 8490732]

13. Naughton M, Dinan TG & Scott LV Corticotropin-releasing hormone and the hypothalamic-pituitary-adrenal axis in psychiatric disease. Handb. Clin. Neurol 124, 69–91 (2014). [PubMed: 25248580]

14. Krashes MJ et al. Rapid, reversible activation of AgRP neurons drives feeding behavior in mice. J. Clin. Invest 121, 1424–1428 (2011). [PubMed: 21364278]

15. Yang CF et al. Sexually dimorphic neurons in the ventromedial hypothalamus govern mating in both sexes and aggression in males. Cell 153, 896–909 (2013). [PubMed: 23663785]

16. Cardoso F et al. Neuro-mesenchymal units control ILC2 and obesity via a brain-adipose circuit. Nature 597, 410–414 (2021). [PubMed: 34408322]

17. Zhang X et al. Brain control of humoral immune responses amenable to behavioural modulation. Nature 581, 204–208 (2020). [PubMed: 32405000]

18. Heidt T et al. Chronic variable stress activates hematopoietic stem cells. Nat. Med 20, 754–758 (2014). [PubMed: 24952646]

19. Mendez-Ferrer S, Lucas D, Battista M & Frenette PS Haematopoietic stem cell release is regulated by circadian oscillations. Nature 452, 442–447 (2008). [PubMed: 18256599]

20. Scheiermann C et al. Adrenergic nerves govern circadian leukocyte recruitment to tissues. Immunity 37, 290–301 (2012). [PubMed: 22863835]

21. Qing H et al. Origin and function of stress-induced IL-6 in murine models. Cell 182, 372–387 (2020). [PubMed: 32610084]

22. Zhao Z et al. A central catecholaminergic circuit controls blood glucose levels during stress. Neuron 95, 138–152 (2017). [PubMed: 28625488]

23. Abe C et al. C1 neurons mediate a stress-induced anti-inflammatory reflex in mice. Nat. Neurosci 20, 700–707 (2017). [PubMed: 28288124]

24. Girbl T et al. Distinct compartmentalization of the chemokines CXCL1 and CXCL2 and the atypical receptor ACKR1 determine discrete stages of neutrophil diapedesis. Immunity 49, 1062–1076 (2018). [PubMed: 30446388]

25. Kohler A et al. G-CSF-mediated thrombopoietin release triggers neutrophil motility and mobilization from bone marrow via induction of Cxcr2 ligands. Blood 117, 4349–4357 (2011). [PubMed: 21224471]

26. Wengner AM, Pitchford SC, Furze RC & Rankin SM The coordinated action of G-CSF and ELR + CXC chemokines in neutrophil mobilization during acute inflammation. Blood 111, 42–49 (2008). [PubMed: 17928531]

27. Eash KJ, Greenbaum AM, Gopalan PK & Link DC CXCR2 and CXCR4 antagonistically regulate neutrophil trafficking from murine bone marrow. J. Clin. Invest 120, 2423–2431 (2010). [PubMed: 20516641]

28. Divangahi M et al. Impact of IL-10 on diaphragmatic cytokine expression and contractility during *Pseudomonas* infection. Am. J. Respir. Cell Mol. Biol 36, 504–512 (2007). [PubMed: 17122368]

29. Divangahi M et al. Lack of CFTR in skeletal muscle predisposes to muscle wasting and diaphragm muscle pump failure in cystic fibrosis mice. PLoS Genet. 5, e1000586 (2009). [PubMed: 19649303]

30. Ayling OG, Harrison TC, Boyd JD, Goroshkov A & Murphy TH Automated light-based mapping of motor cortex by photoactivation of channelrhodopsin-2 transgenic mice. Nat. Methods 6, 219–224 (2009). [PubMed: 19219033]

31. Arenkiel BR et al. In vivo light-induced activation of neural circuitry in transgenic mice expressing channelrhodopsin-2. Neuron 54, 205–218 (2007). [PubMed: 17442243]

32. Economo MN et al. Distinct descending motor cortex pathways and their roles in movement. Nature 563, 79–84 (2018). [PubMed: 30382200]

33. Kawai R et al. Motor cortex is required for learning but not for executing a motor skill. Neuron 86, 800–812 (2015). [PubMed: 25892304]

34. Xie X et al. Single-cell transcriptome profiling reveals neutrophil heterogeneity in homeostasis and infection. Nat. Immunol 21, 1119–1133 (2020). [PubMed: 32719519]

35. Xu C, Lee SK, Zhang D & Frenette PS The gut microbiome regulates psychological-stress-induced inflammation. Immunity 53, 417–428 (2020). [PubMed: 32735844]

36. Viswanathan K & Dhabhar FS Stress-induced enhancement of leukocyte traf icking into sites of surgery or immune activation. Proc. Natl Acad. Sci. USA 102, 5808–5813 (2005). [PubMed: 15817686]

37. Rangachari M & Kuchroo VK Using EAE to better understand principles of immune function and autoimmune pathology. J. Autoimmun 45, 31–39 (2013). [PubMed: 23849779]

38. Winkler ES et al. SARS-CoV-2 infection of human ACE2-transgenic mice causes severe lung in lammation and impaired function. Nat. Immunol 21, 1327–1335 (2020). [PubMed: 32839612]

39. King IL et al. Intestinal helminth infection impacts the systemic distribution and function of the naive lymphocyte pool. Mucosal Immunol. 10, 1160–1168 (2017). [PubMed: 28120841]

40. Elftman MD et al. Stress-induced glucocorticoids at the earliest stages of herpes simplex virus-1 infection suppress subsequent antiviral immunity, implicating impaired dendritic cell function. J. Immunol 184, 1867–1875 (2010). [PubMed: 20089700]

41. Briganti A, Barsotti G, Portela DA, Di Nieri C & Breghi G Effects of rocuronium bromide on globe position and respiratory function in iso lurane-anesthetized dogs: a comparison between three different dosages. Vet. Ophthalmol 18, 89–94 (2015). [PubMed: 24131770]

42. Dobin A et al. STAR: ultrafast universal RNA-seq aligner. Bioinformatics 29, 15–21 (2013). [PubMed: 23104886]

43. Anders S, Pyl PT & Huber W HTSeq–a Python framework to work with high-throughput sequencing data. Bioinformatics 31, 166–169 (2015). [PubMed: 25260700]

44. Robinson MD, McCarthy DJ & Smyth GK edgeR: a Bioconductor package for differential expression analysis of digital gene expression data. Bioinformatics 26, 139–140 (2010). [PubMed: 19910308]

45. Anders S et al. Count-based differential expression analysis of RNA sequencing data using R and Bioconductor. Nat. Protoc 8, 1765–1786 (2013). [PubMed: 23975260]

46. Butler A, Hoffman P, Smibert P, Papalexi E & Satija R Integrating single-cell transcriptomic data across different conditions, technologies, and species. Nat. Biotechnol 36, 411–420 (2018). [PubMed: 29608179]

47. Haghverdi L, Lun ATL, Morgan MD & Marioni JC Batch effects in single-cell RNA-sequencing data are corrected by matching mutual nearest neighbors. Nat. Biotechnol 36, 421–427 (2018). [PubMed: 29608177]
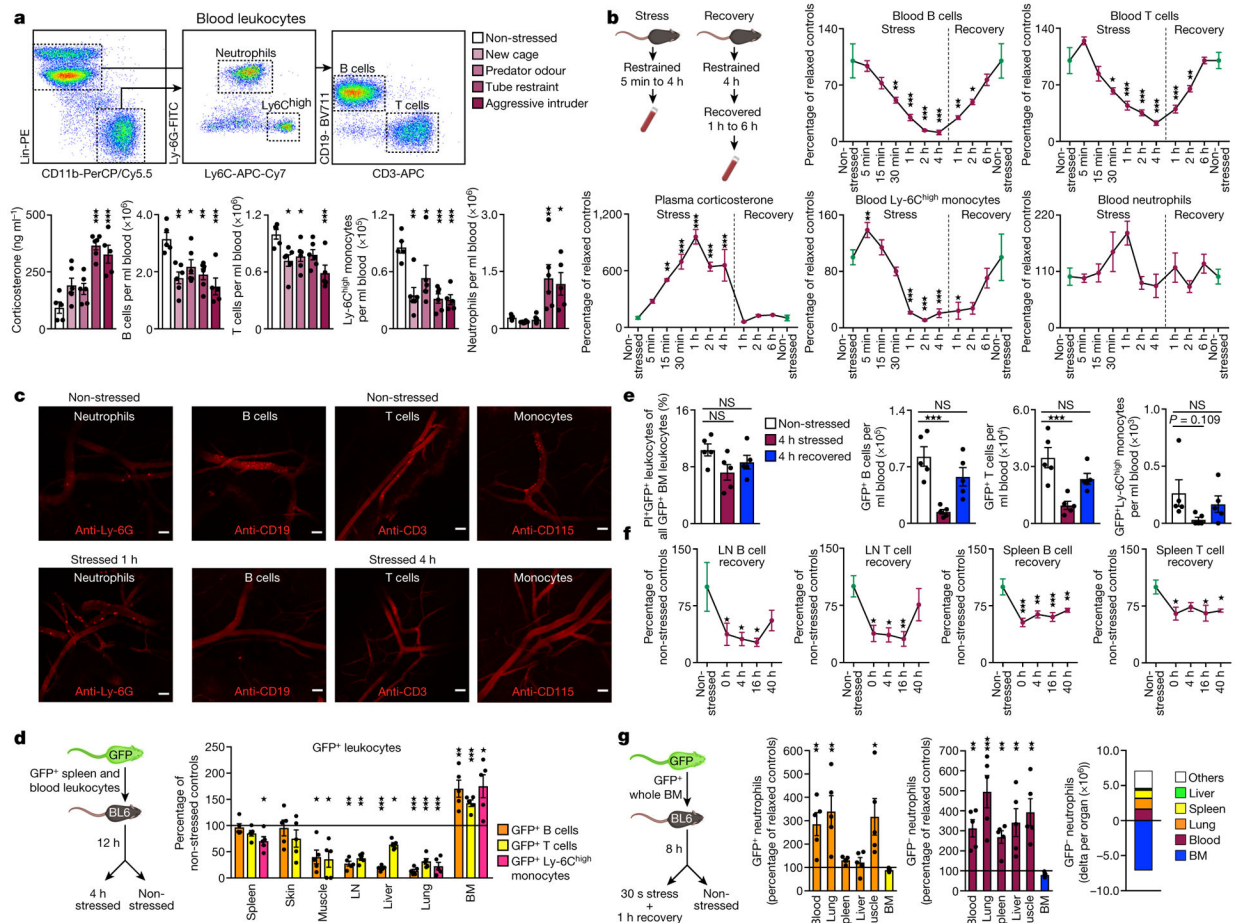
Fig. 1 |. Acute psychological stress induces leukocyte shifts.

a, The gating strategy and the indicated measurements in mice exposed to psychological stressors for 1 h. $n = 5$ (non-stressed and aggressive intruder) and $n = 6$ (new cage, predator odour and tube restraint) mice. **b**, Blood leukocytes and plasma corticosterone levels measured at the indicated times. 'Stress' indicates the timepoint directly after restraint stress. $n = 4$ mice per timepoint. 'Recovery' indicates the timepoint after the indicated time of recovery from a 4 h restraint. $n = 4$ mice per timepoint. **c**, Intravital microscopy of blood leukocyte populations after the indicated stress durations. Scale bar, 50 μm. **d**, Experimental schematic and quantification of transferred GFP+ leukocytes in different organs. $n = 5$ mice per group. **e**, Assessment of cell death of transferred GFP+ leukocytes in the bone marrow and quantification of GFP+ leukocytes in the blood of recipient mice under the indicated conditions. $n = 5$ mice per group. **f**, B cell and T cell numbers in inguinal lymph nodes (LN) and spleen measured after the indicated time of recovery from one 4 h restraint stress episode. $n = 4$ (non-stressed LN analyses) and $n = 5$ (other analyses) mice. **g**, Experimental schematic and quantification of transferred GFP+ and endogenous GFP− neutrophils in different organs expressed as a percentage of the mean neutrophil number in the respective organ in non-stressed control mice. $n = 6$ (non-stressed) and $n = 5$ (stressed) mice. Estimated body-wide total loss of endogenous GFP− neutrophils from the bone marrow plotted against estimated total gain of endogenous GFP− neutrophils in most

relevant peripheral destinations. For **a**, **b** and **d**–**g**, data are mean ± s.e.m. Statistical analysis was performed using one-way analysis of variance (ANOVA) (**a**, **b**, **e** and **f**) and two-tailed unpaired *t*-tests (**d** and **g**); ★*P* < 0.05, ★★*P* < 0.01, ★★★*P* < 0.001.
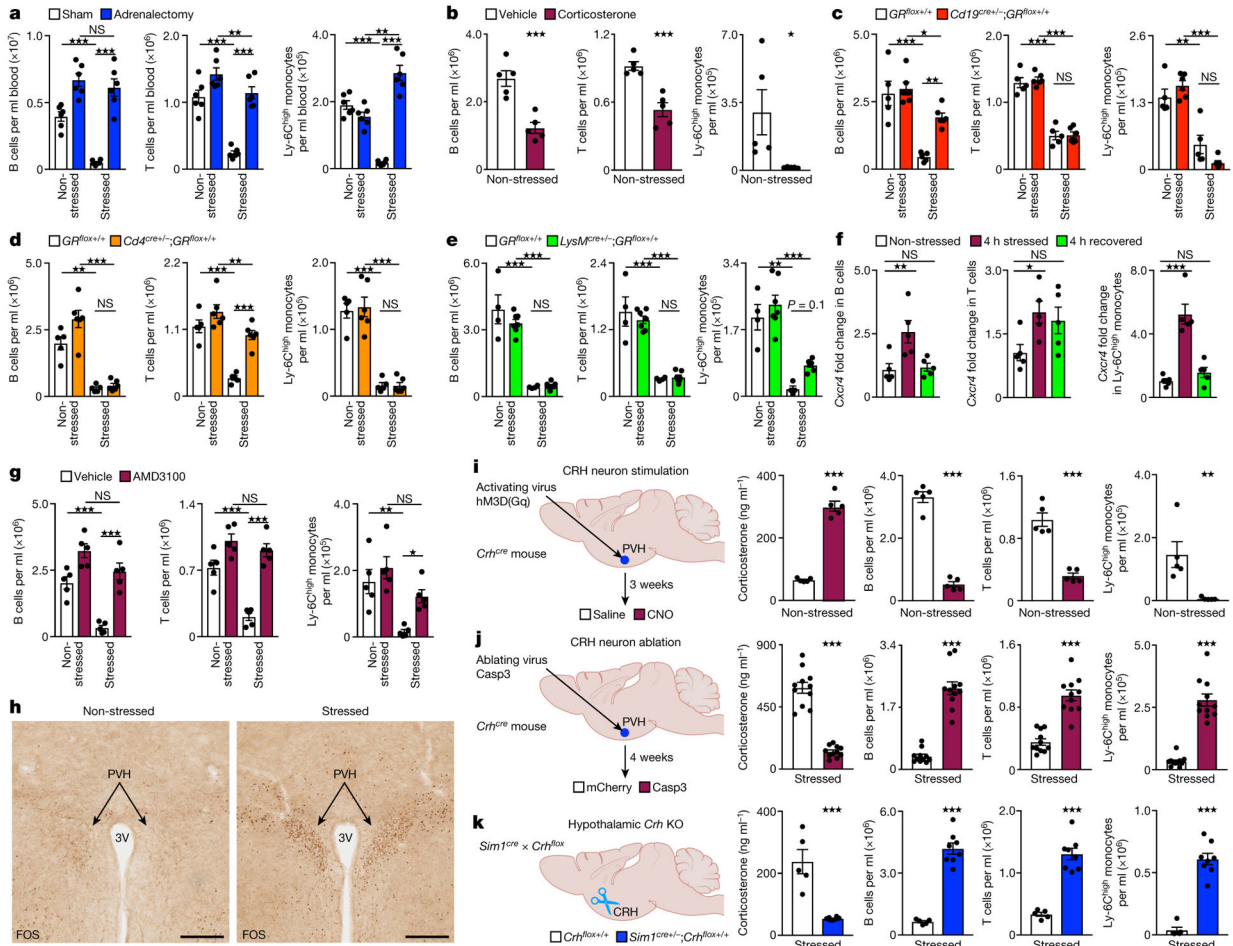
Fig. 2 |. The PVH controls leukocyte homing to the bone marrow during stress.
a, Blood leukocytes in the indicated groups at the baseline and after 4 h of restraint. $n = 6$ mice per group. **b**, Blood leukocytes after injection of vehicle or corticosterone into wild-type (WT) mice. $n = 5$ mice per group. **c–e**, Blood leukocytes of mice with B-cell-specific ($n = 5$ (control) and $n = 6$ (KO) mice) (**c**), T-cell-specific ($n = 5$ (controls) and $n = 6$ (KO) mice) (**d**) and myeloid-specific ($n = 4$ (control) and $n = 7$ (KO) mice) (**e**) KO of the GR at the baseline and after 4 h of restraint. **f**, Transcript expression of *Cxcr4* in sorted blood leukocytes of WT mice under the indicated conditions. $n = 5$ mice per group. **g**, Blood leukocytes in WT mice that were injected with CXCR4 inhibitor versus vehicle under the indicated conditions. $n = 4$ groups, $n = 5$ mice per group. AMD3100 or vehicle was injected intraperitoneally 30 min before stress onset. Control mice injected with AMD3100 and vehicle remained non-stressed until bleeding at 4.5 h after injection. **h**, Immunohistological staining of FOS^{+} neurons in the PVH of non-stressed control mice and restraint-stressed mice. 3V, third ventricle. Scale bars, 200 μm. **i**, Experimental schematic, plasma corticosterone and circulating leukocytes 5 h after intraperitoneal injection of clozapine-*N*-oxide (CNO) or vehicle. $n = 5$ mice per group. **j**, Experimental schematic, plasma corticosterone and circulating leukocytes in response to a 4 h restraint episode in mice injected with Caspase-3 virus versus mCherry-control virus. Total from two combined experiments; $n = 11$ mice per group. **k**, Experimental schematic, plasma corticosterone and

circulating leukocytes in response to a 4 h restraint episode in hypothalamic *Crh*-KO mice ($n = 8$ (*Sim1$^{cre+/-}$;Crh$^{flox+/+}$*)) and control mice ($n = 5$ (*Crh$^{flox+/+}$*)). For **a–g** and **i–k**, data are mean ± s.e.m. Statistical analysis was performed using one-way (**f**) and two-way (**a, c, d, e** and **g**) ANOVA, and two-tailed unpaired *t*-tests (**b** and **i–k**); ★$P < 0.05$, ★★$P < 0.01$, ★★★$P < 0.001$.
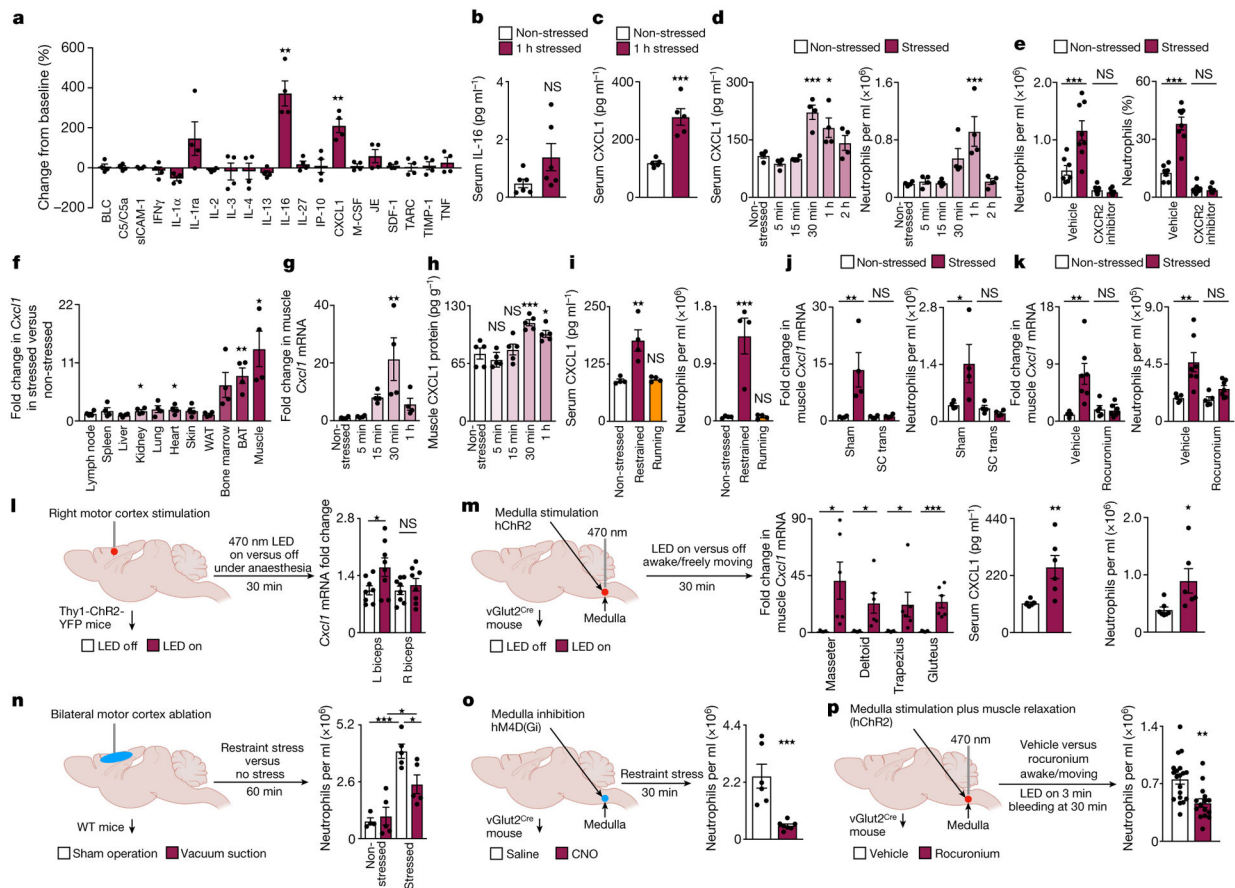
Fig. 3 |. Central motor circuits control neutrophil egress from the bone marrow during acute stress.

a, Plasma cytokines after 1 h restraint. $n = 4$ mice per group. **b**, IL-16 serum levels. $n = 6$ mice per group. **c**, CXCL1 serum levels. $n = 5$ mice per group. **d**, CXCL1 serum levels and blood neutrophil numbers after restraint. $n = 4$ mice per group. **e**, Blood neutrophils in mice treated with vehicle versus CXCR2 inhibitor under non-stressed conditions and after 1 h restraint. $n = 7$–8 mice per group. **f**, Transcript expression of *Cxcl1* in different organs after 30 min of restraint. $n = 4$ mice per group. **g**, *Cxcl1* expression in gluteal muscle after the indicated restraint durations. $n = 4$ mice per group. **h**, CXCL1 protein in skeletal muscle. $n = 5$ mice per group. **i**, Serum CXCL1 and blood neutrophil numbers after 1 h restraint versus voluntary running. $n = 4$ mice per group. **j**, *Cxcl1* expression in gluteal muscle and blood neutrophil numbers in spinal-cord-transected (SC trans) mice after 30 min restraint. $n = 4$ mice per group. **k**, *Cxcl1* expression in gluteal muscle and blood neutrophil numbers in mice that were treated with muscle relaxant (rocuronium) 15 min after a 3 min restraint stress episode. $n = 4$–7 per group. **l**, Experimental schematic and *Cxcl1* expression in the left (L) and right (R) biceps muscles in the indicated groups. Two experiments combined; total $n = 8$ mice per group. **m**, Experimental schematic, *Cxcl1* expression in the indicated muscles, serum CXCL1 protein and blood neutrophil numbers in the indicated groups. $n = 6$–7 per group. **n**, Experimental schematic and blood neutrophil numbers under the indicated conditions. $n = 4$–5 per group. **o**, Experimental schematic and neutrophil numbers in the indicated groups. $n = 6$–7 per group. **p**, Experimental schematic and neutrophil numbers in

the indicated groups. Two experiments with changed groups combined; $n = 15$ and 19 mice per group. For **a**–**p**, data are mean ± s.e.m. Statistical analysis was performed using one-way (**d** and **g**–**i**) and two-way (**e**, **j**–**l** and **n**) ANOVA, and two-tailed unpaired t-tests (**a**–**c**, **f**, **m**, **o** and **p**); ★$P < 0.05$, ★★$P < 0.01$, ★★★$P < 0.001$.
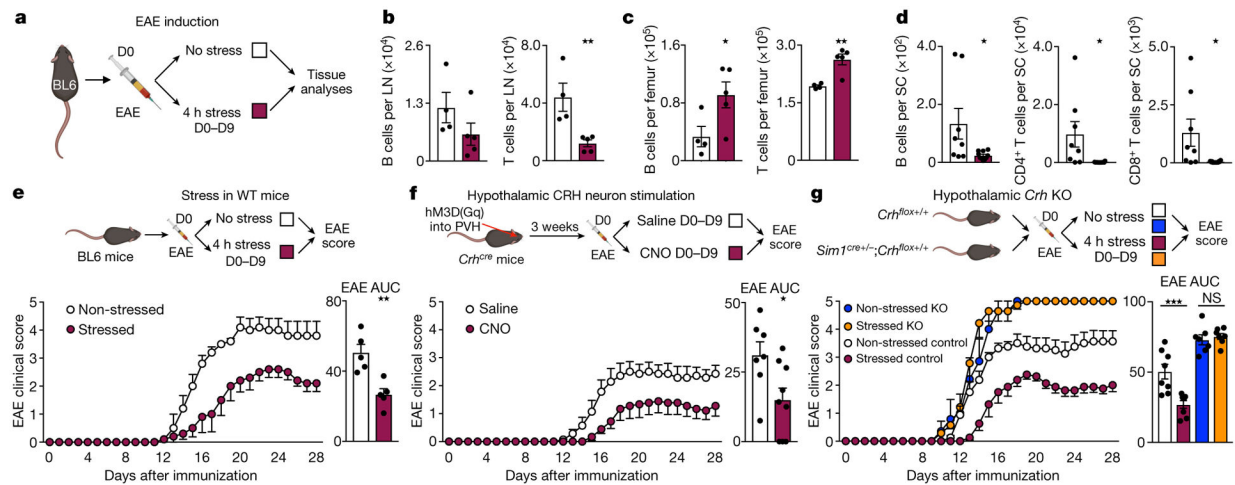
Fig. 4 |. Acute stress protects against the acquisition of autoimmunity.

a, Experimental schematic. **b,c**, Quantification of IgD^{+} B cells and T cells in the inguinal lymph nodes (**b**) and bone marrow (**c**) in the indicated groups. $n = 4$ (non-stressed) and $n = 5$ (stressed) mice. **d**, Quantification of leukocytes in the spinal cord (SC) in the indicated groups 14 d after EAE induction. $n = 8$ (non-stressed) and $n = 10$ (stressed) mice. **e**, Experimental schematic and EAE clinical score in the indicated groups. $n = 5$ (non-stressed) and $n = 5$ (stressed) mice. Area under the curve (AUC) of the EAE clinical score. **f**, Experimental schematic and EAE clinical score in the indicated groups. $n = 7$ (saline-injected) and $n = 9$ (CNO-injected) mice; two experiments combined. AUC of the EAE clinical score. **g**, Experimental schematic and EAE clinical score in the indicated groups. $n = 8$ (non-stressed $Crh^{flox+/+}$ control), $n = 8$ (stressed $Crh^{flox+/+}$ control), $n = 7$ (non-stressed $Sim1^{cre+/-};Crh^{flox+/+}$ KO) and $n = 7$ (stressed $Sim1^{cre+/-};Crh^{flox+/+}$ KO) mice. AUC of the EAE clinical score. For **b**–**g**, data are mean ± s.e.m. Statistical analysis was performed using two-way ANOVA (**g**)) and two-tailed unpaired t-tests (**b**–**f**); ★$P < 0.05$, ★★$P < 0.01$, ★★★$P < 0.001$.
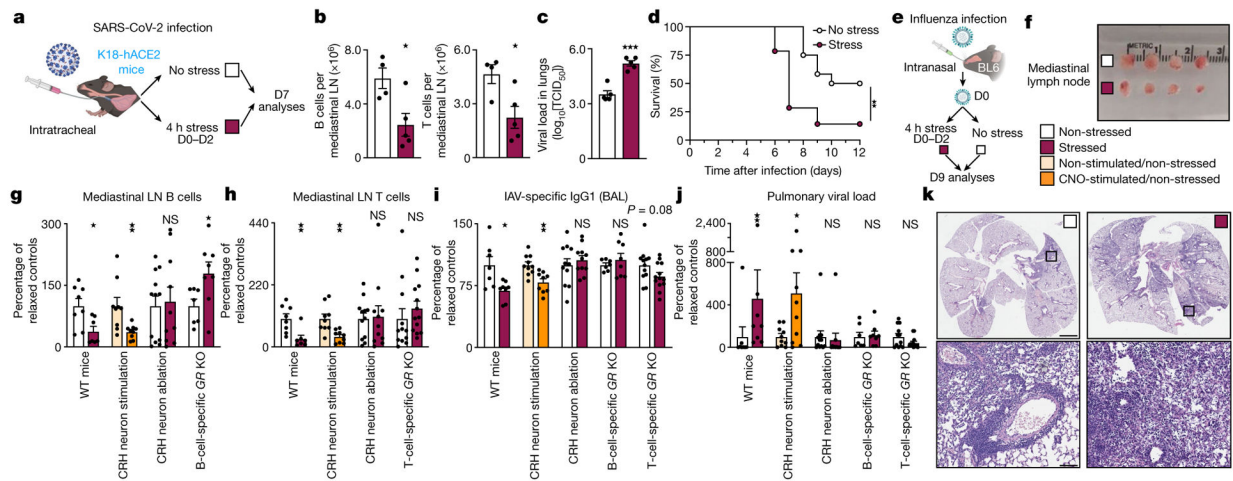
Fig. 5 |. Acute stress impairs the acquisition of immunity to SARS-CoV-2 and influenza.
a, Experimental schematic. **b**, Lymphocytes in the lymph nodes. $n = 4–5$ mice per group.
c, Pulmonary viral loads. $n = 5$ mice per group. **d**, Survival curves. $n = 12$ (non-stressed)
and $n = 14$ (stressed) mice; two experiments. **e–k**, Mice were infected with a sublethal dose
of IAV. **e**, Experimental schematic. **f**, Images of the mediastinal lymph nodes. **g**, B cells in
the mediastinal lymph nodes of WT, PVH CRH-neuron-ablated and B-cell-specific *GR*-KO
mice, as well as of mice with chemogenetic PVH-CRH neuron stimulation (dark orange) or
vehicle injection (light orange). $n = 7–12$ mice per group. **h**, T cells in the mediastinal lymph
nodes in mice as described above and indicated, except for T-cell-specific *GR*-KO mice. $n = 7–13$ mice per group. **i,j**, IAV-specific IgG1 in the BAL (**i**) and pulmonary viral loads (**j**)
of mice as described above and as indicated. $n = 7–13$ mice per group. **k**, Haematoxylin
and eosin-stained lung cross-sections of mice under the indicated conditions. Scale bars, 1
mm (low magnification) and 41 μm (high magnification). For **b**, **c** and **g–j**, data are mean
± s.e.m. Statistical analysis was performed using two-tailed unpaired *t*-tests (**b**, **c** and **g–i**),
log-rank (Mantel–Cox) tests (**d**) and two-tailed unpaired *t*-tests and Mann–Whitney *U*-tests
(**j**); ★$P < 0.05$, ★★$P < 0.01$, ★★★$P < 0.001$.